Supplementary Materials

3D μEFPocket for Multimodal Communications with Brain Organoids

Yihang Wang[1#], Miguel A. Cuevas[2#], Zhihan Zhang[3#], Gooyoon Chung[1#], Jingze Zhang[1], Yilan Yin[2], Qianzhi Luo[4], Will Lipman[5], Josh Henderson[4], Lucas Lu[6], Weixiang Zeng[4], Anran Zhang[1], Changxin Jia[1], Haiwen Luan[3,7*], Jason L. Stein[2*], and Wubin Bai[1*]

[1]Department of Applied Physical Sciences, University of North Carolina at Chapel Hill, Chapel Hill, NC, 27514, USA

[2]Department of Genetics and UNC Neuroscience Center, University of North Carolina at Chapel Hill, Chapel Hill, NC, 27514, USA

[3]Department of Mechanical and Aerospace Engineering, University of California San Diego, La Jolla, CA 92093, USA

[4]UNC/NCSU Joint Department of Biomedical Engineering

[5]Department of Psychology and Neuroscience, University of North Carolina at Chapel Hill, Chapel Hill, NC, 27514, USA

[6]Department of Biology, University of North Carolina at Chapel Hill, Chapel Hill, NC, 27514, USA

[7]Program in Materials Science and Engineering, University of California San Diego, La Jolla, CA 92093, USA

[#]These authors contributed equally: Yihang Wang, Miguel A. Cuevas, Zhihan Zhang, Gooyoon Chung

*Corresponding authors: Wubin Bai (email: wbai@unc.edu), Jason L. Stein (email: jason_stein@med.unc.edu), Haiwen Luan (email: h2luan@ucsd.edu)

Contents

No.	Name	Abbreviation	Functionalities	Design purpose
1	Microfluidic test device-1	μFTest-1	Mesh-like microfluidic channels	Geometrical and mechanical test of 3D microfluidics
2	Microfluidic test device-2	μFTest-2	6 microfluidic channels	Geometrical and mechanical test of 3D microfluidics
3	Microelectrofluidic test device-1	μEFTest-1	2 microfluidic channels + 4 thermal resisters	Geometrical and mechanical test of 3D microelectrofluidics
4	Microfluidic Pocket-1	μFPocket-1	8 microfluidic channels	Multichannel 3D microfluidics for organoid chemical delivery
5	Microfluidic Pocket-2	μFPocket-2	6 microfluidic channels	Multichannel 3D conformal microfluidics for organoid chemical delivery
6	Microfluidic Pocket-3	μFPocket-3	6 microfluidic channels	Multichannel 3D conformal microfluidics for organoid chemical delivery
7	Microfluidic Pocket-4	μFPocket-4	6 microfluidic channels	Multichannel 3D microfluidics for organoid chemical delivery
8	Microfluidic Pocket-5	μFPocket-5	8 microfluidic channels	Multichannel 3D microfluidics for organoid chemical delivery
9	Microelectrofluidic Pocket-1	μEFPocket-1	3 microfluidic channels + 84 microelectronic channels	Multichannel 3D microelectrofluidics for organoid chemical delivery and electrical stimulation
10	Microelectrofluidic Pocket-2	μEFPocket-2	3 microfluidic channels + 96 microelectronic channels	Multichannel 3D microelectrofluidics for organoid chemical delivery and electrical stimulation
11	Microelectrofluidic Pocket-3	μEFPocket-3	3 microfluidic channels + 18 microelectronic channels	Multichannel 3D microelectrofluidics for organoid chemical delivery and electrical stimulation

Table S1. List of microfluidic and microelectrofluidic devices.

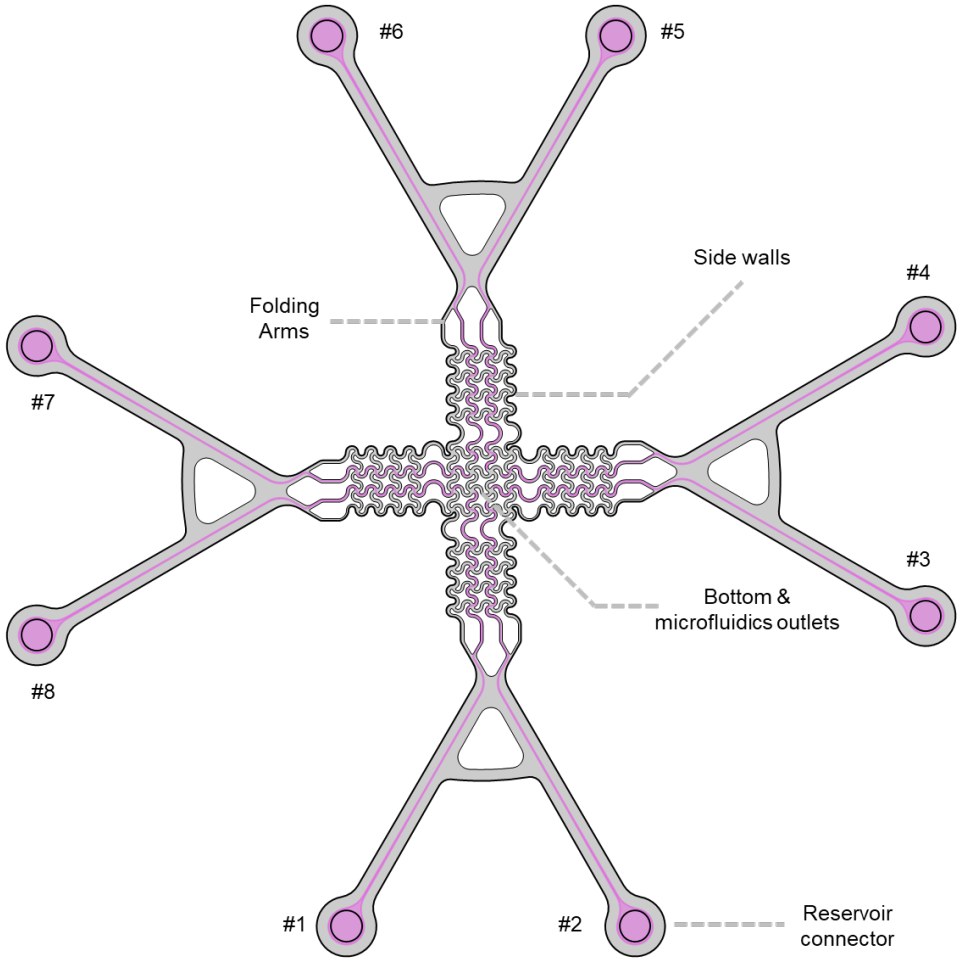

Figure S1. Two-dimensional structures of μFPocket-1. Layers (microfluidics and PPX-C) are labeled in different colors.

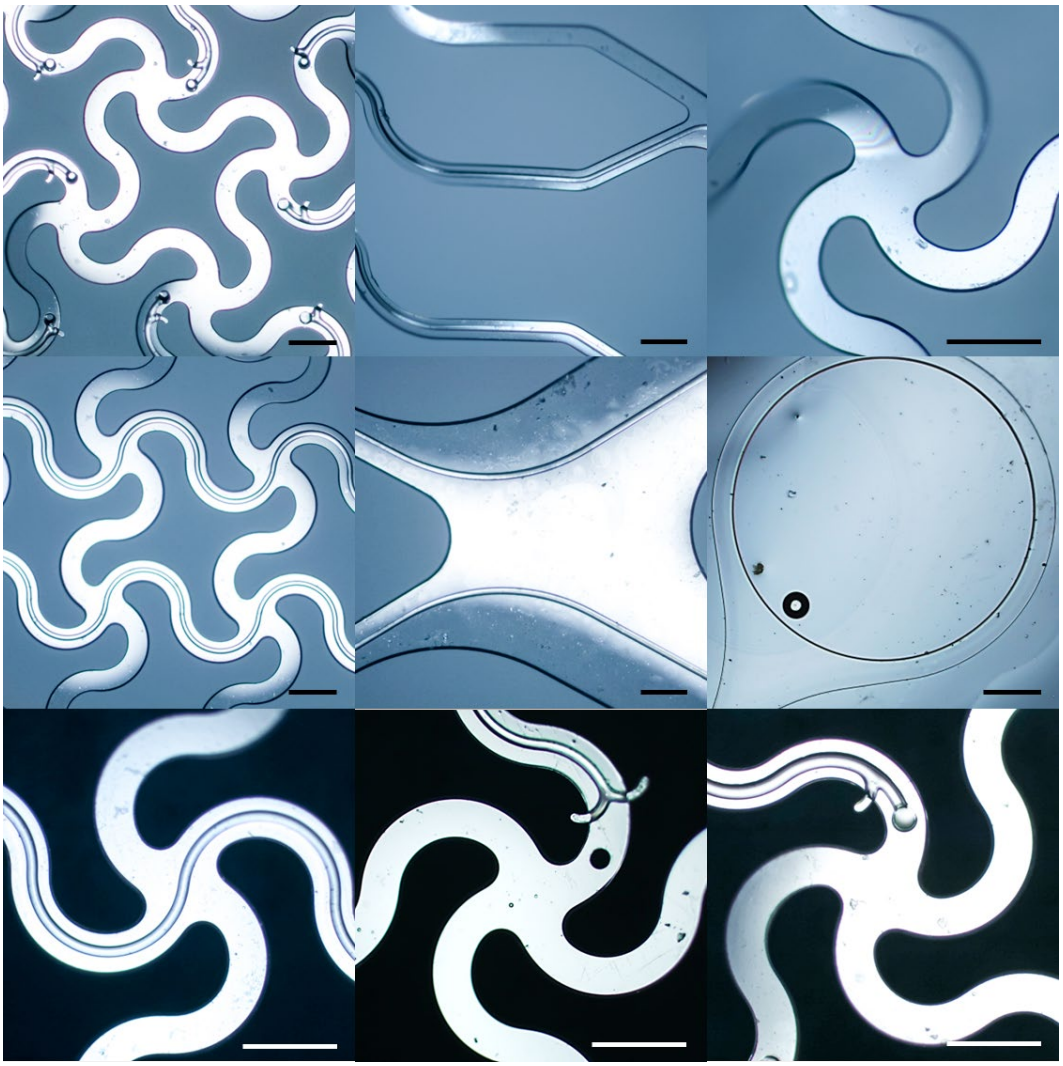

Figure S2. Optical images of μFPocket-1. Scale bars: 250 μm.

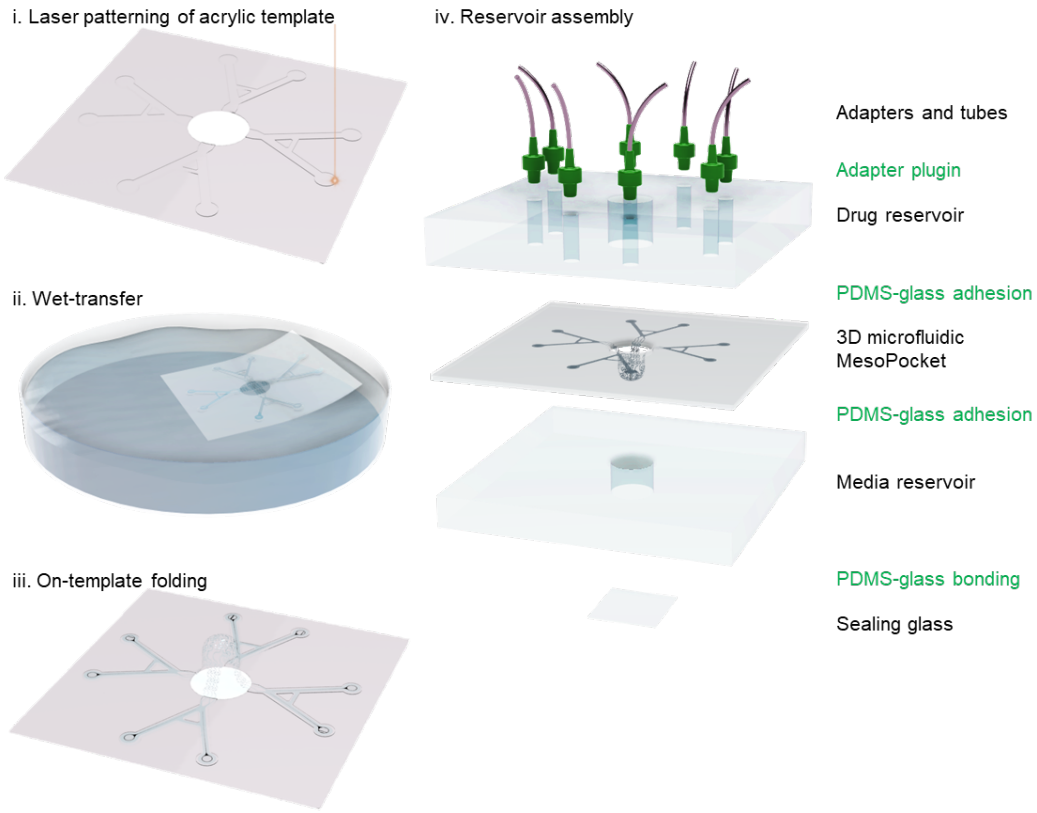

Figure S3. Schematic illustrations of the μFPocket-1 3D assembly. Step i-iv show the post-fabrication assembly process of microfluidics. Drug and media reservoirs are made of PDMS.

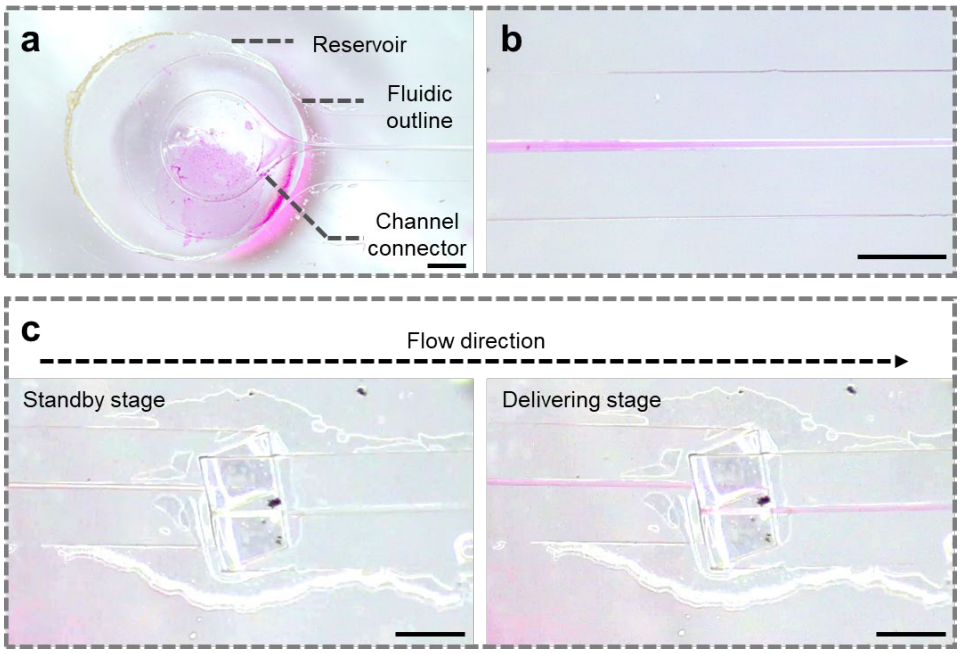

Figure S4. Reliability and robustness of the μFPocket assembly. a. Fluidic connection between microfluidics and the reservoir. **b.** Encapsulation performance of microfluidics. **c.** Robustness of microfluidics with structure folded after encapsulation. Scale bars: 500 μm.

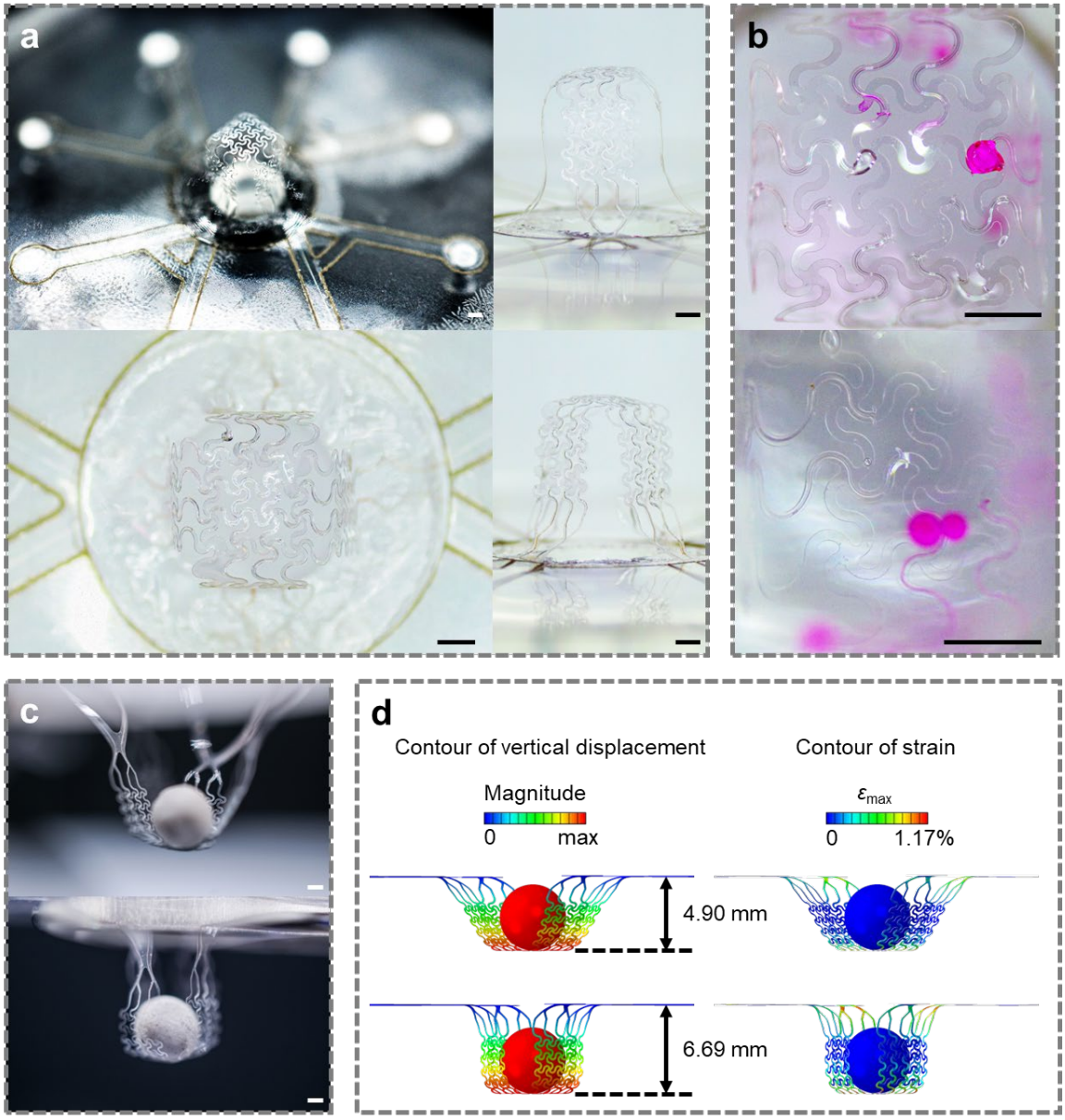

Figure S5. Structure characterizations of 3D folded μFPocket-1 and simulation. a. Optical images of 3D folded μFPocket corresponding to Step iii of **Figure S3** (without drug reservoir). **b.** Optical images of μFPocket-1 delivering dye solution in the air (top) and under water (bottom). **c.** Optical images of μFPocket-1 hosting a spherical organoid phantom at various opening angles. **d.** Finite element analysis of the structure. Scale bars: 1 mm.

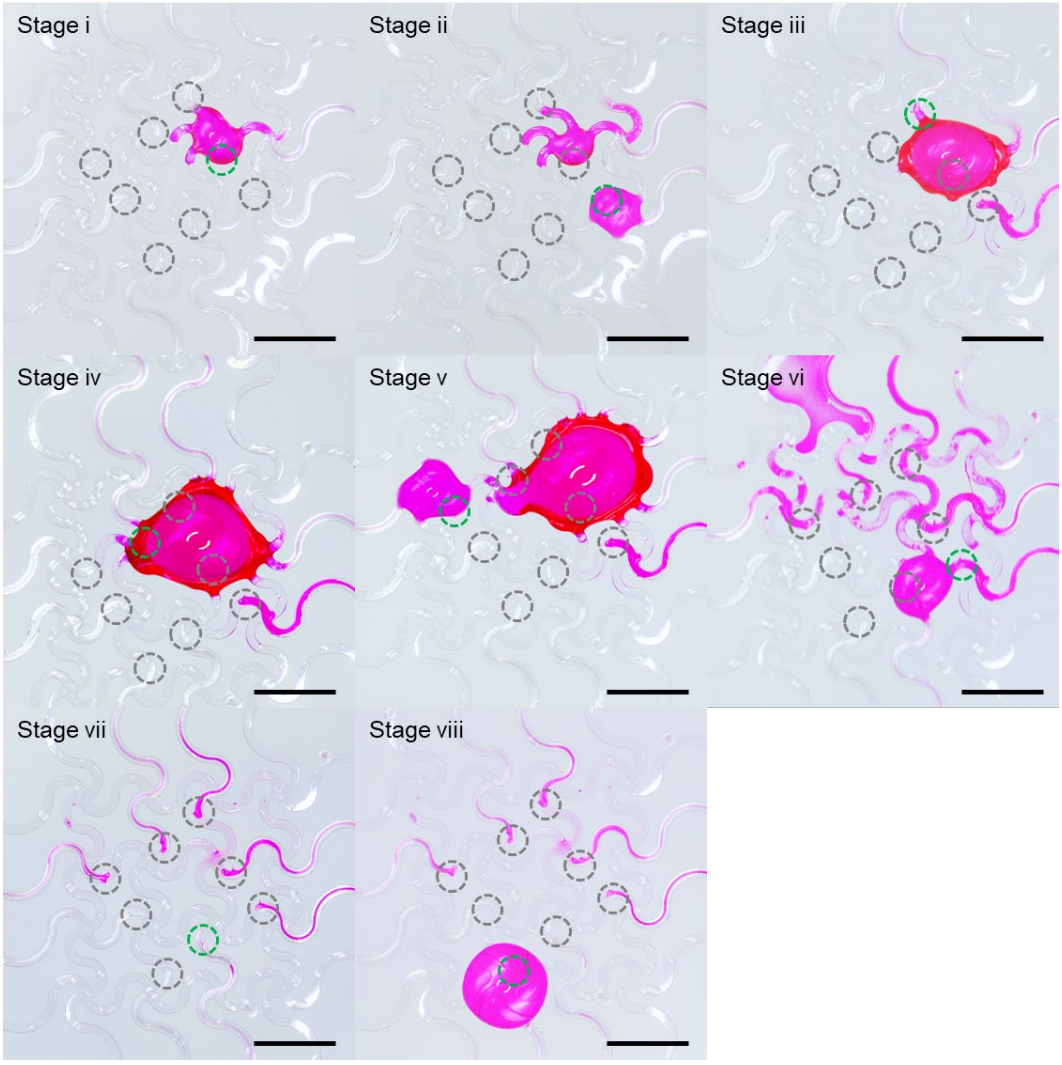

Figure S6. Spatial temporal on-demand drug delivery demonstration of μFPocket-1. Step i-viii show site-specific delivery of dye solution. Microfluidic outlets of working and standby channels are labeled (green: working; grey: standby). This corresponds to **Supplementary Movie 2**. Scale bars: 1 mm.

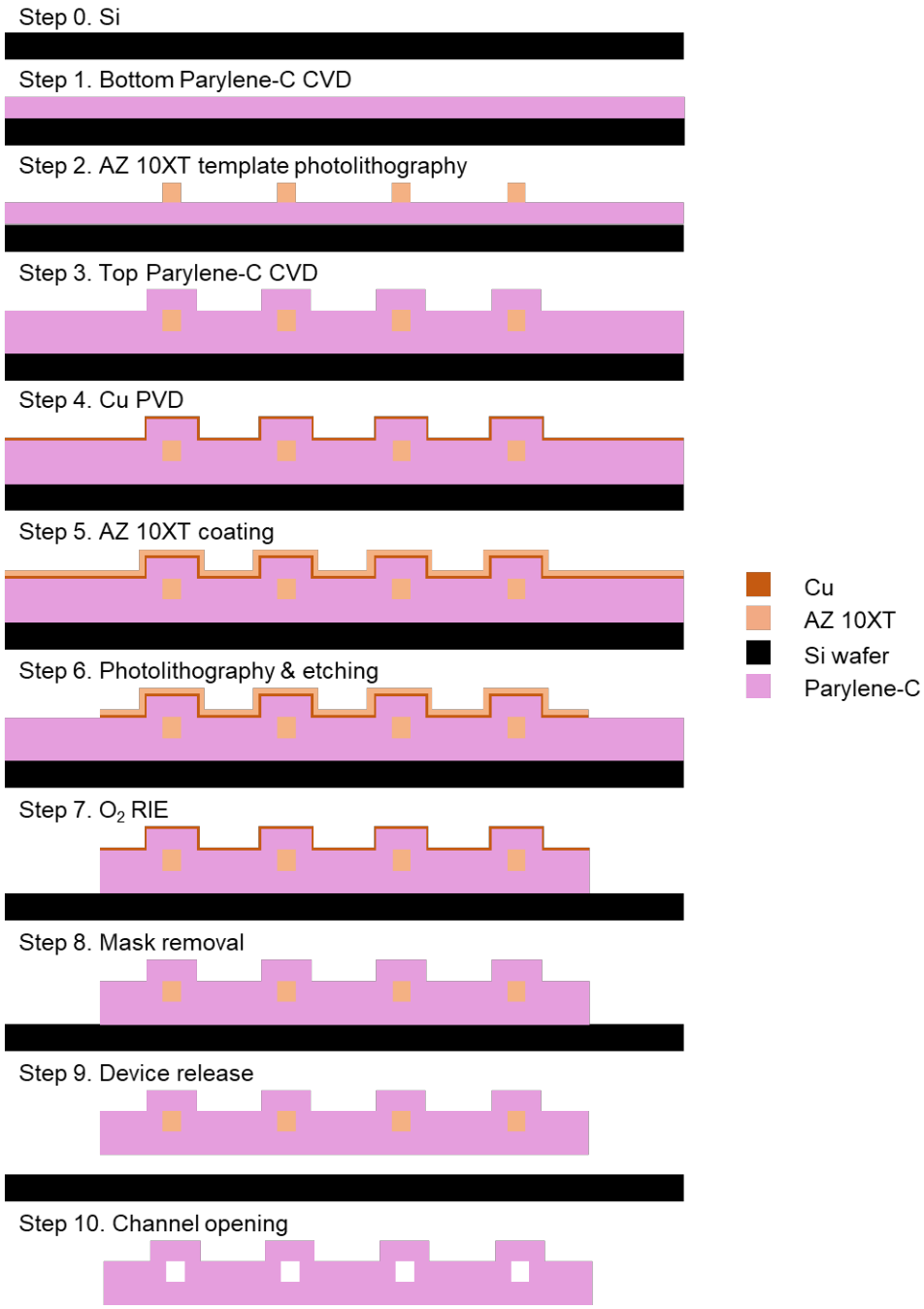

Figure S7. Cross-sectional illustrations of the multi-step fabrication of PPX-C based microfluidics. Layers (Cu, AZ 10XT, Si, and Parylene-C) are labeled in different colors.

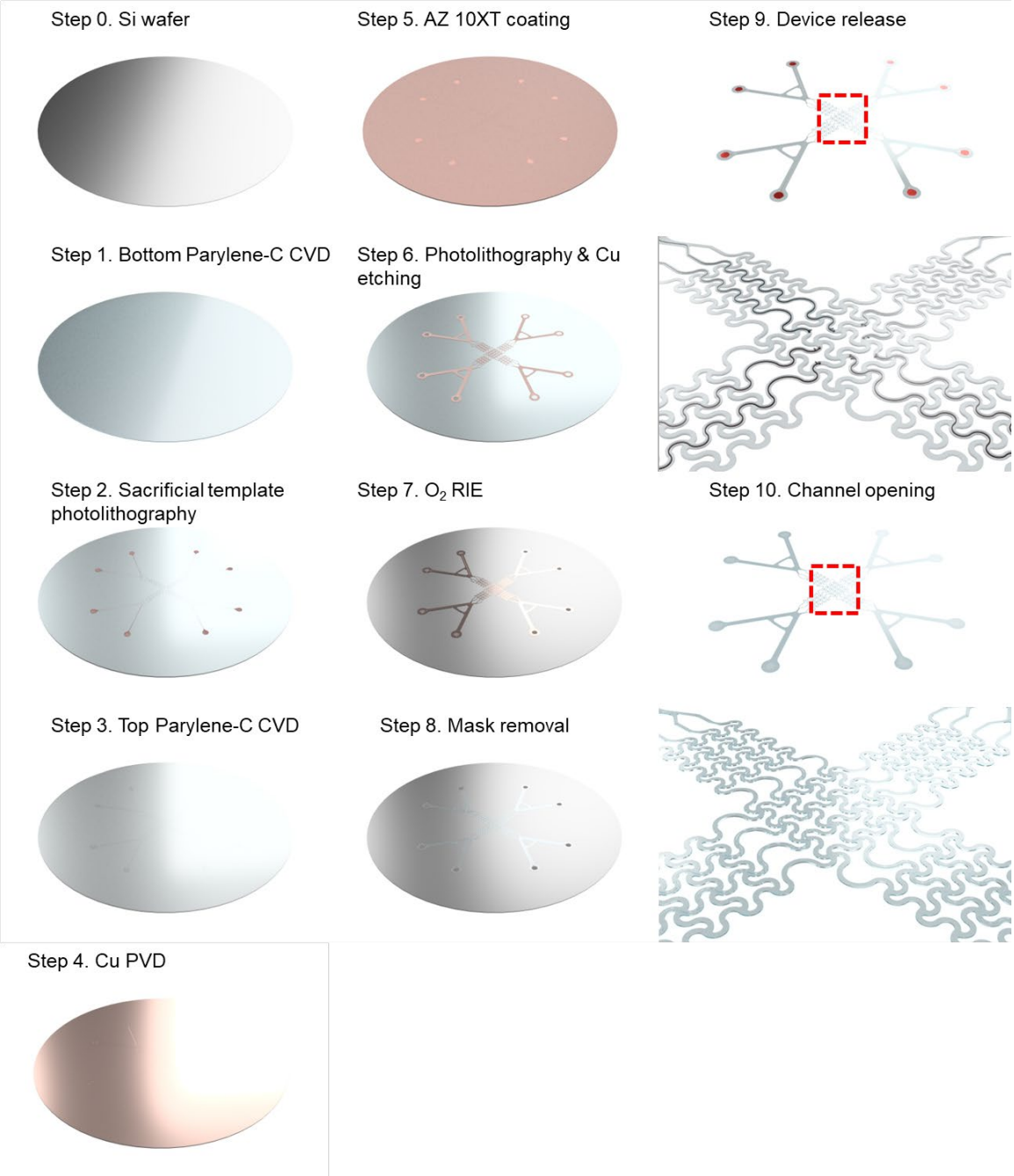

Figure S8. Schematic illustrations of the multi-step fabrication of the 2D precursor of μFPocket-1 corresponding to Figure S7. Step 0-10 show the fabrication of PPX μF (additional closer views of Step 9-10 are attached).

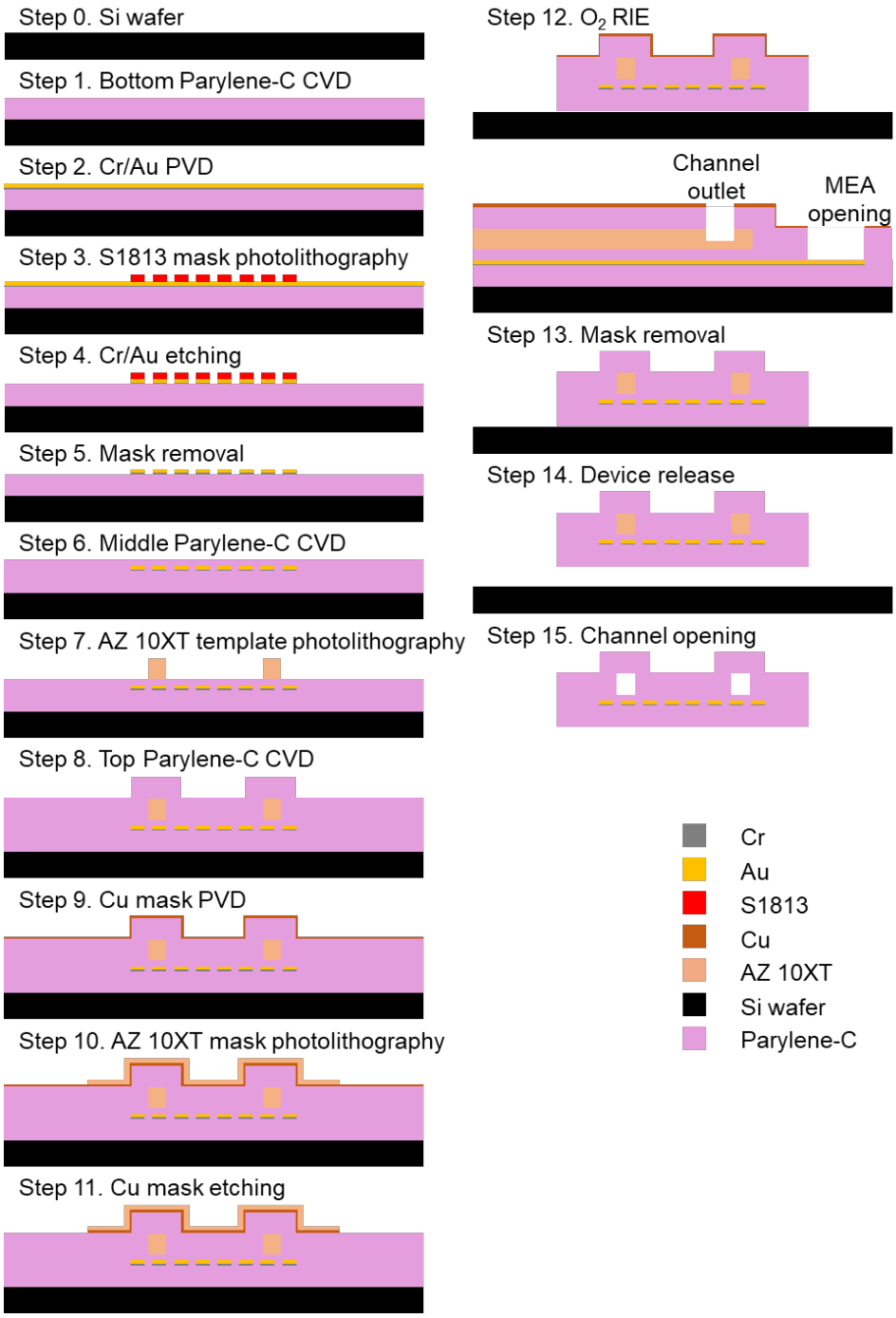

Figure S9. Cross-sectional schematic illustrations of the fabrication of PPX-C based microelectrofluidics. Layers (Cr, Au, S1813, Cu, AZ 10XT, Si, and Parylene-C) are labeled in different colors.

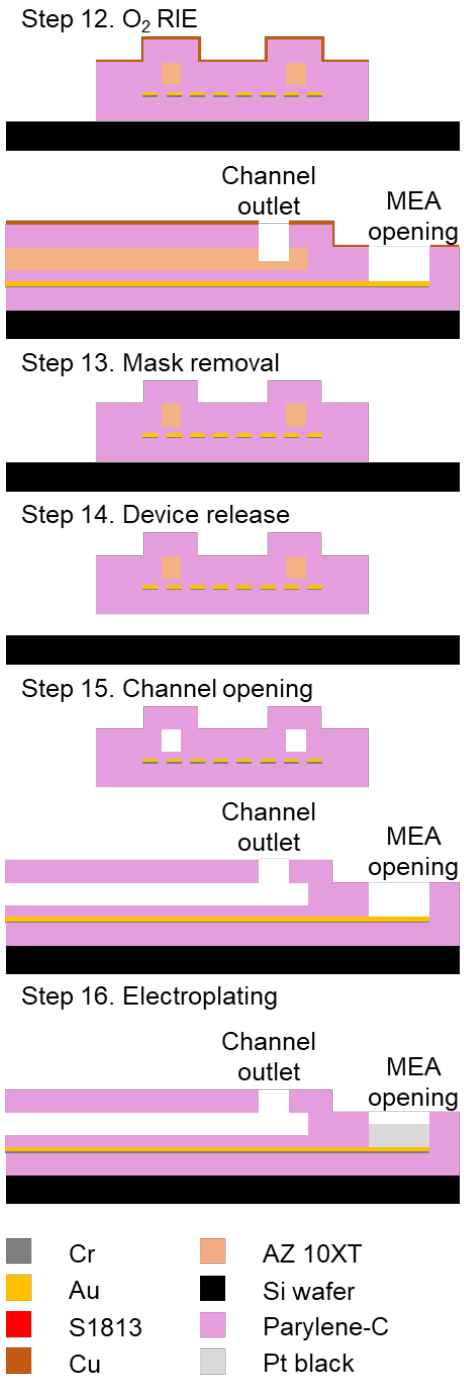

Figure S10. Cross-sectional schematic illustrations of the Pt black (PtB) electroplating. Layers (Cr, Au, S1813, Cu, AZ 10XT, Si, Parylene-C, and Pt black) are labeled in different colors.

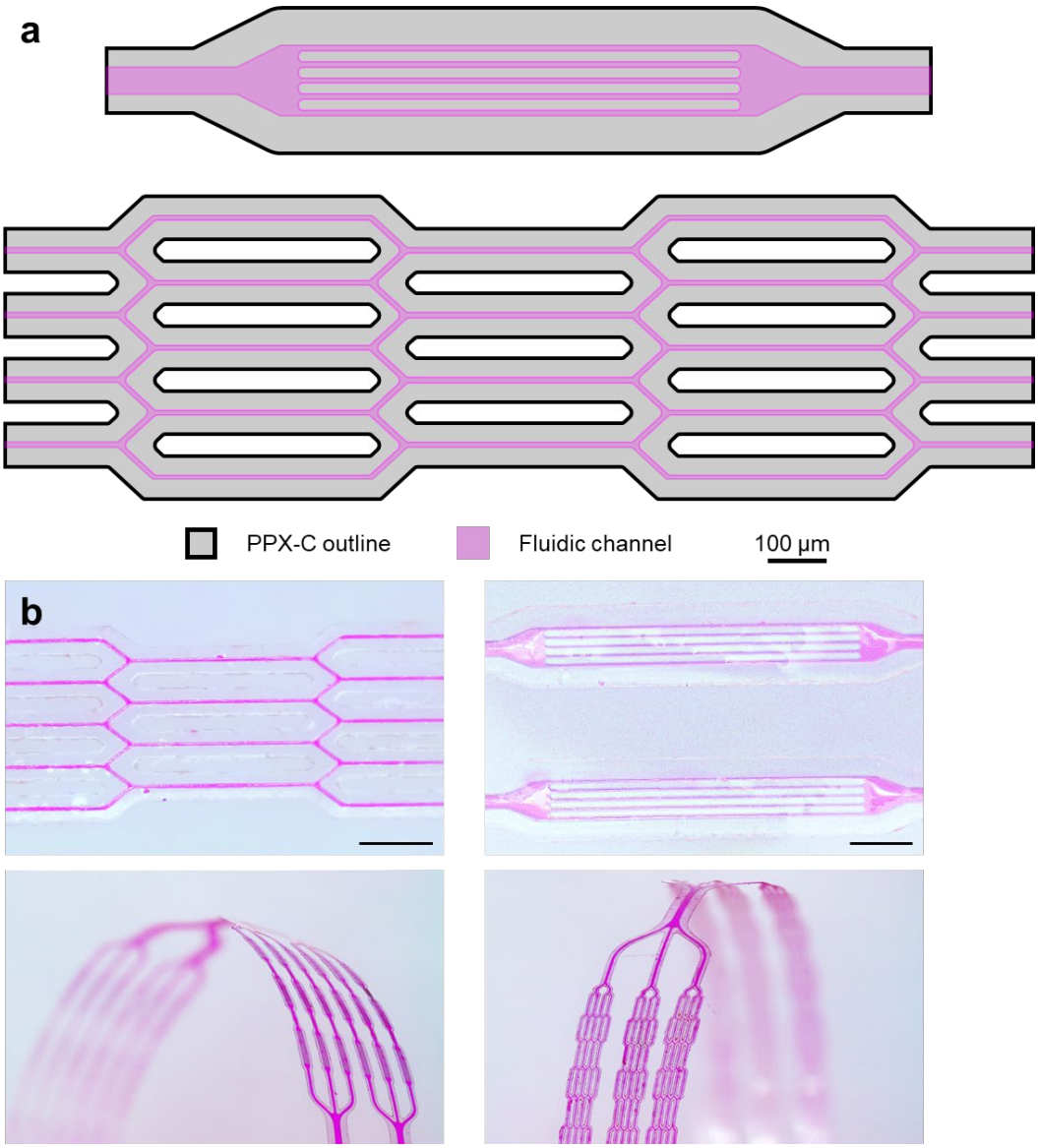

Figure S11. Design of µFTest-1. a. Two-dimensional structures (partial) of mesh-like microfluidic device µFTest-1. Layers (microfluidics, and PPX-C) are labeled in different colors. **b.** Detailed structures of microvascular-like microfluidics. Scale bars: 100 µm in **a**, 200 µm in **b**.

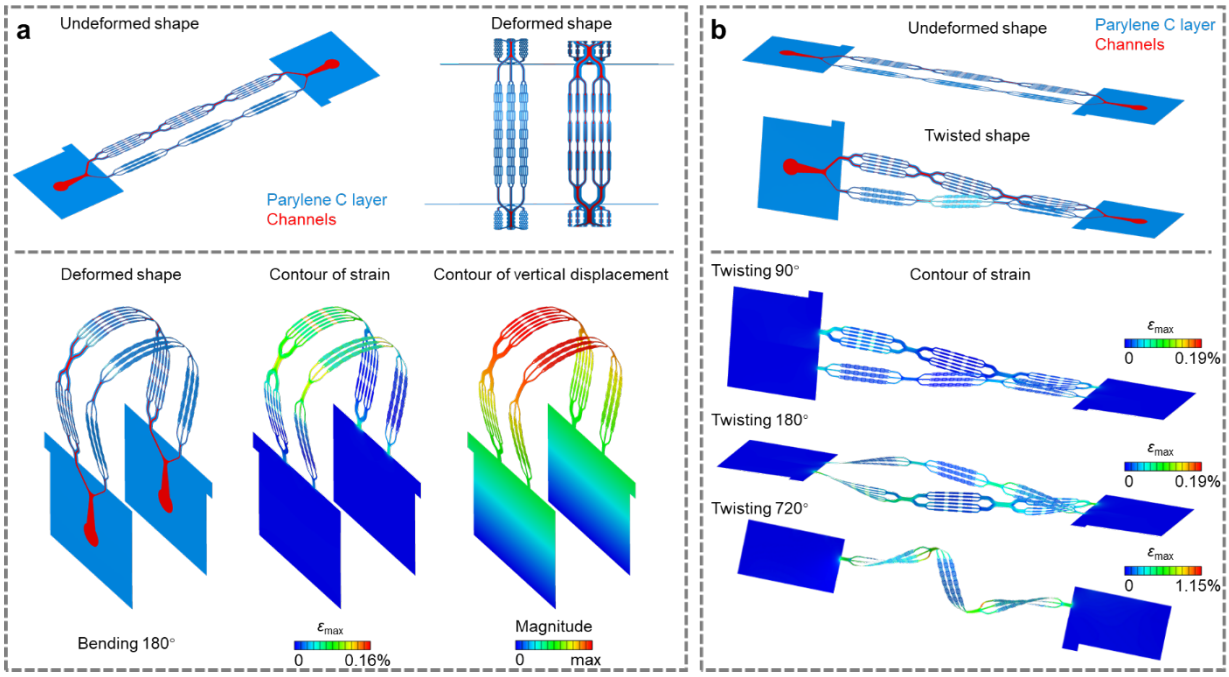

Figure S12. Finite-element analysis of μFTest-1 upon bending (a) and twisting (b).

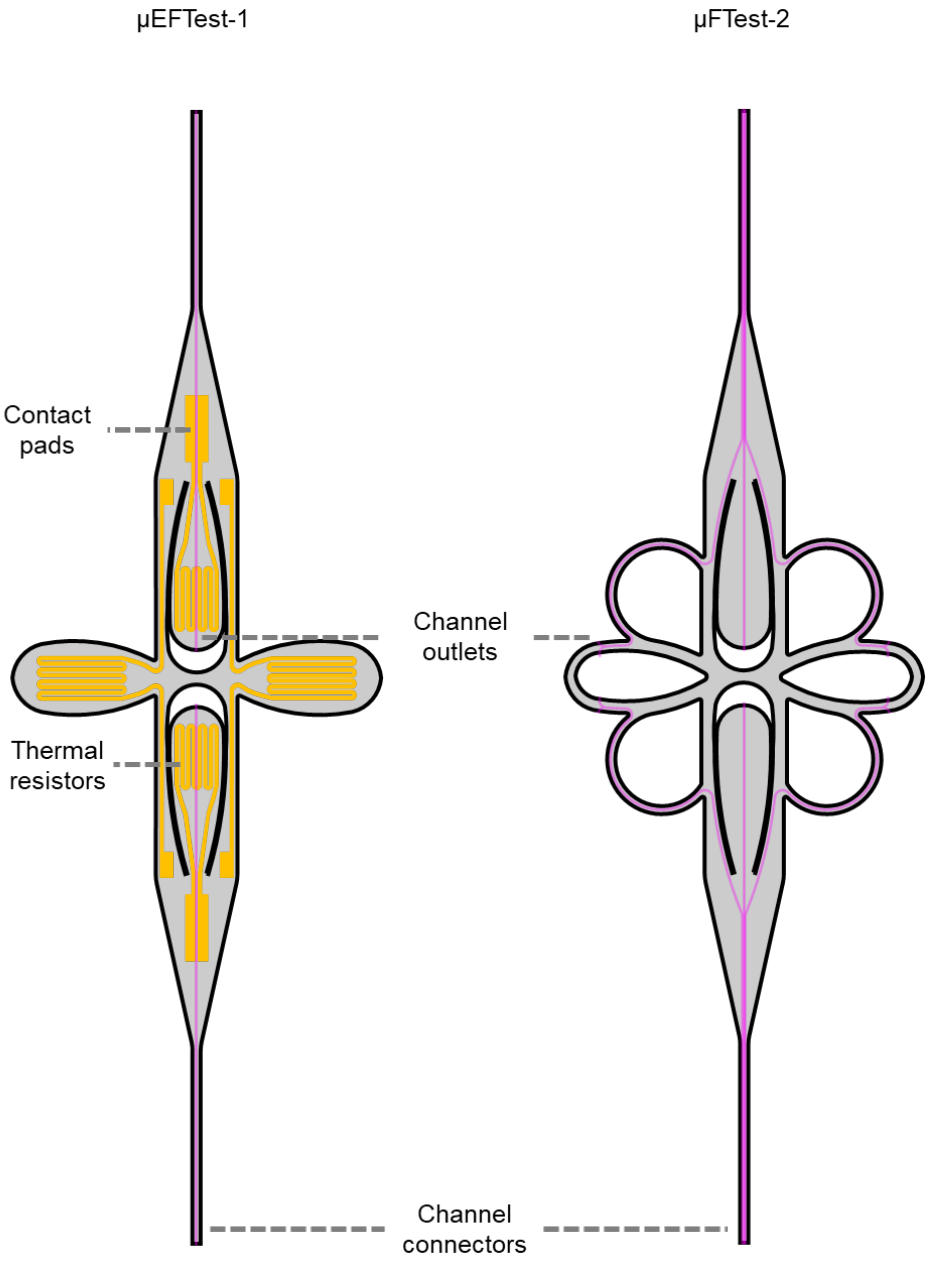

Figure S13. Two-dimensional structures of μFTest-2 and μEFTest-1. Layers (metal, microfluidics, and PPX-C) are labeled in different colors.

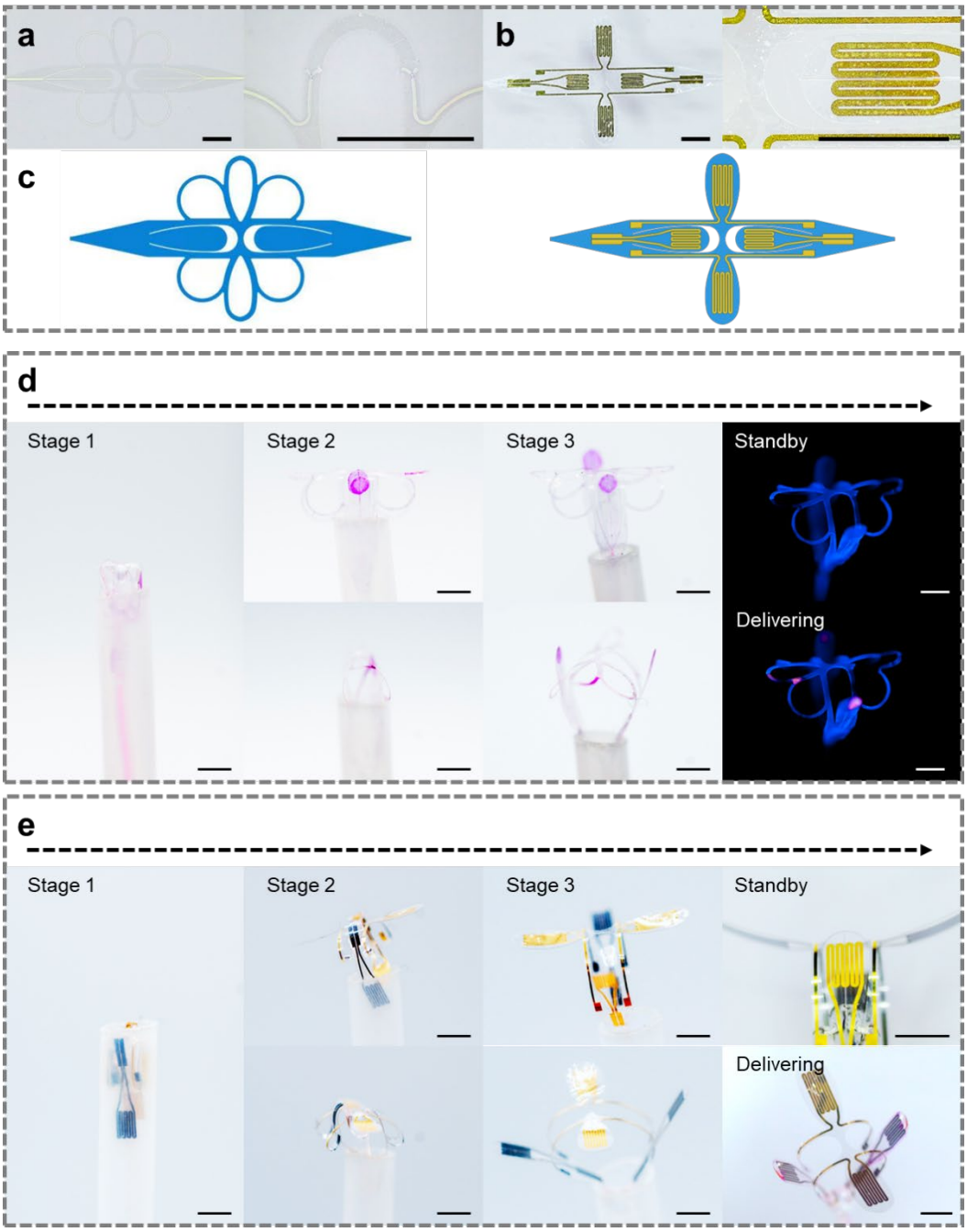

Figure S14. Mechanical tests of μFTest-2 and μEFTest-1. a.-b. Planar structure of μFTest-2 (**a**) and μEFTest-1 (**b**). **c.** Structure of μFTest-2 and μEFTest-1 used in FEA analysis. Blue, Parylene-C; yellow, metal. **d.-e.** Catheter-based structure tests of μFTest-2 (**d**) and μEFTest-1 (**e**). Scale bars: 2 mm.

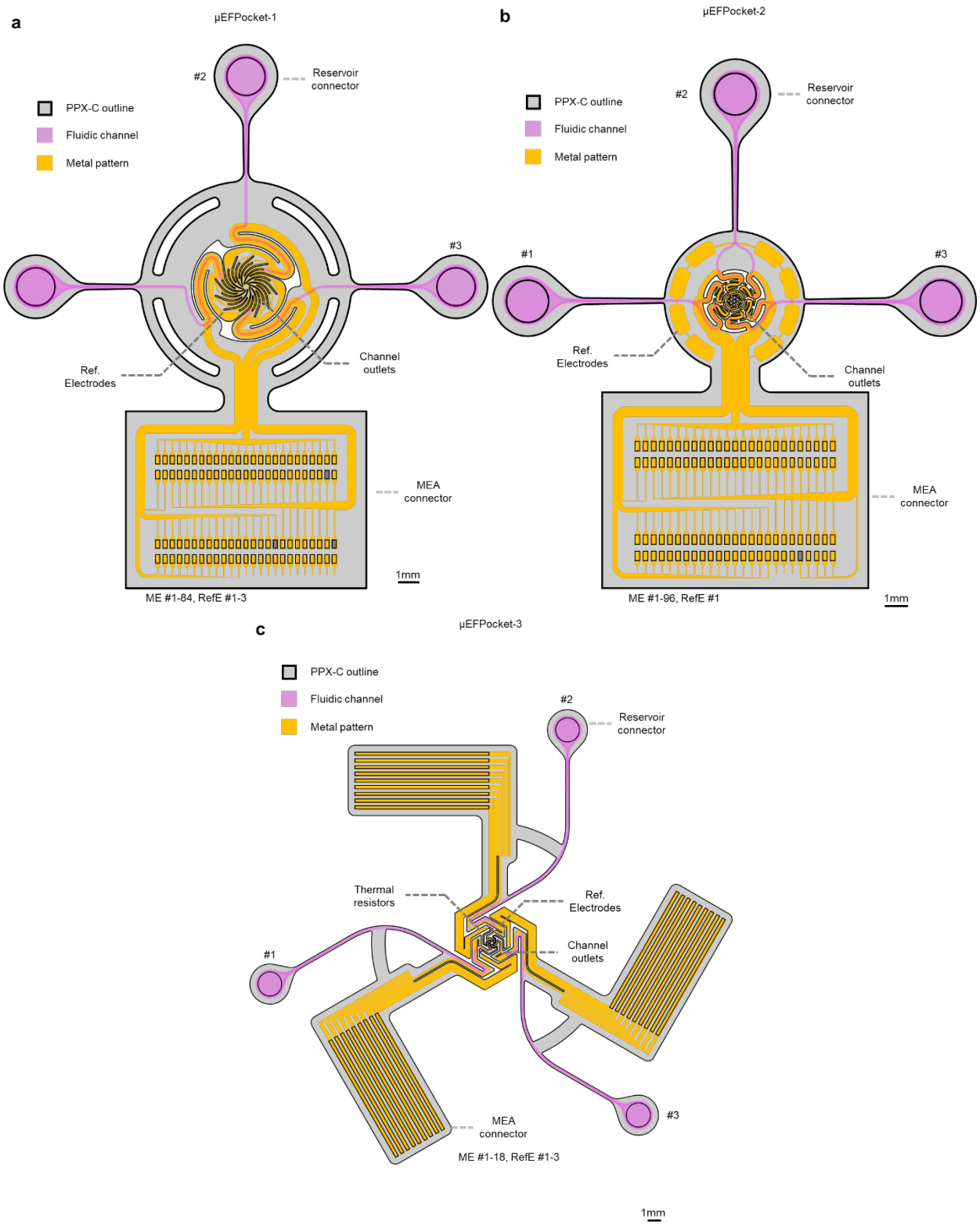

Figure S15. Two-dimensional structures of μEFPocket-1, 2, and 3. Layers (metal, microfluidics, and PPX-C) are labeled in different colors. Microelectrodes and reference electrodes openings are omitted.

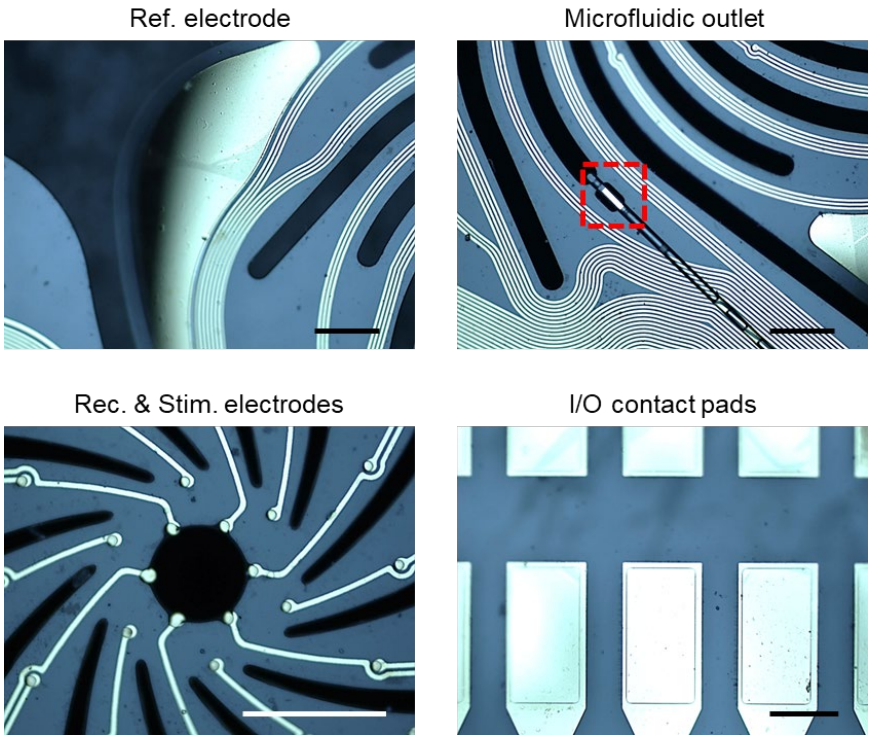

Figure S16. Optical images of μEFPockets. Scale bars: 200 μm.

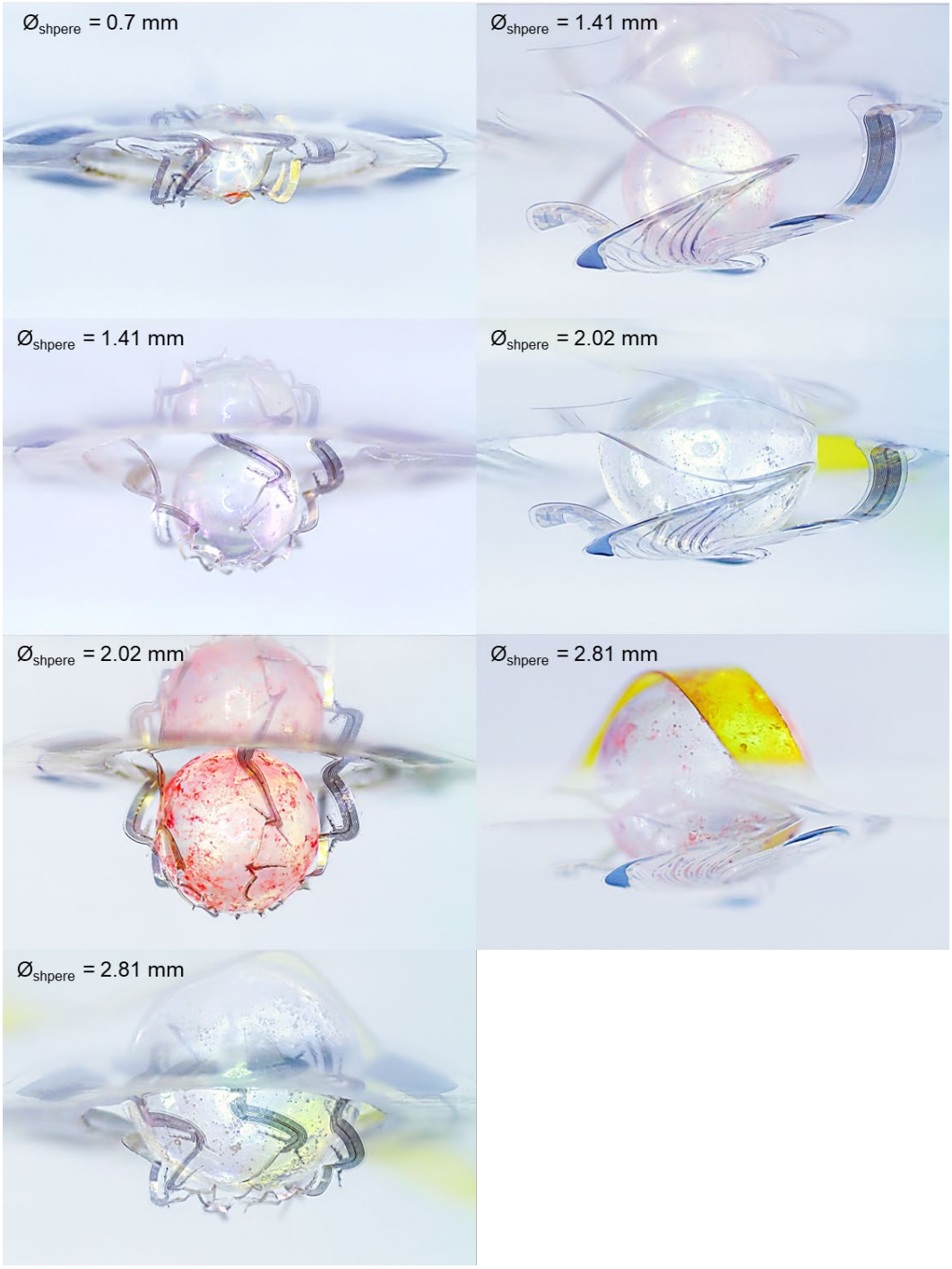

Figure S17. Structure flexibility tests of MEA μEFPocket-1 (right) and 2 (left). Diameters of spheres (Ø$_{shpere}$) are labeled.

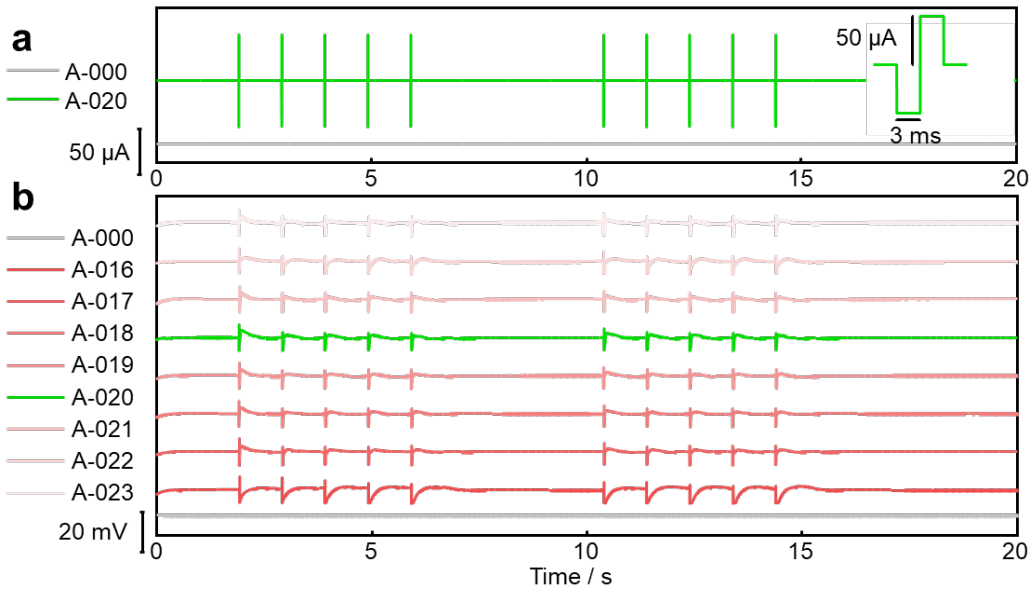

Figure S18. Electrical stimulation test study of MEA in the µEFPocket. a. Electrical stimulation current. **b.** Recording of electrical stimulation. Reference channel (grey), stimulation channel (green), and recording channels (red) are labeled in different colors.

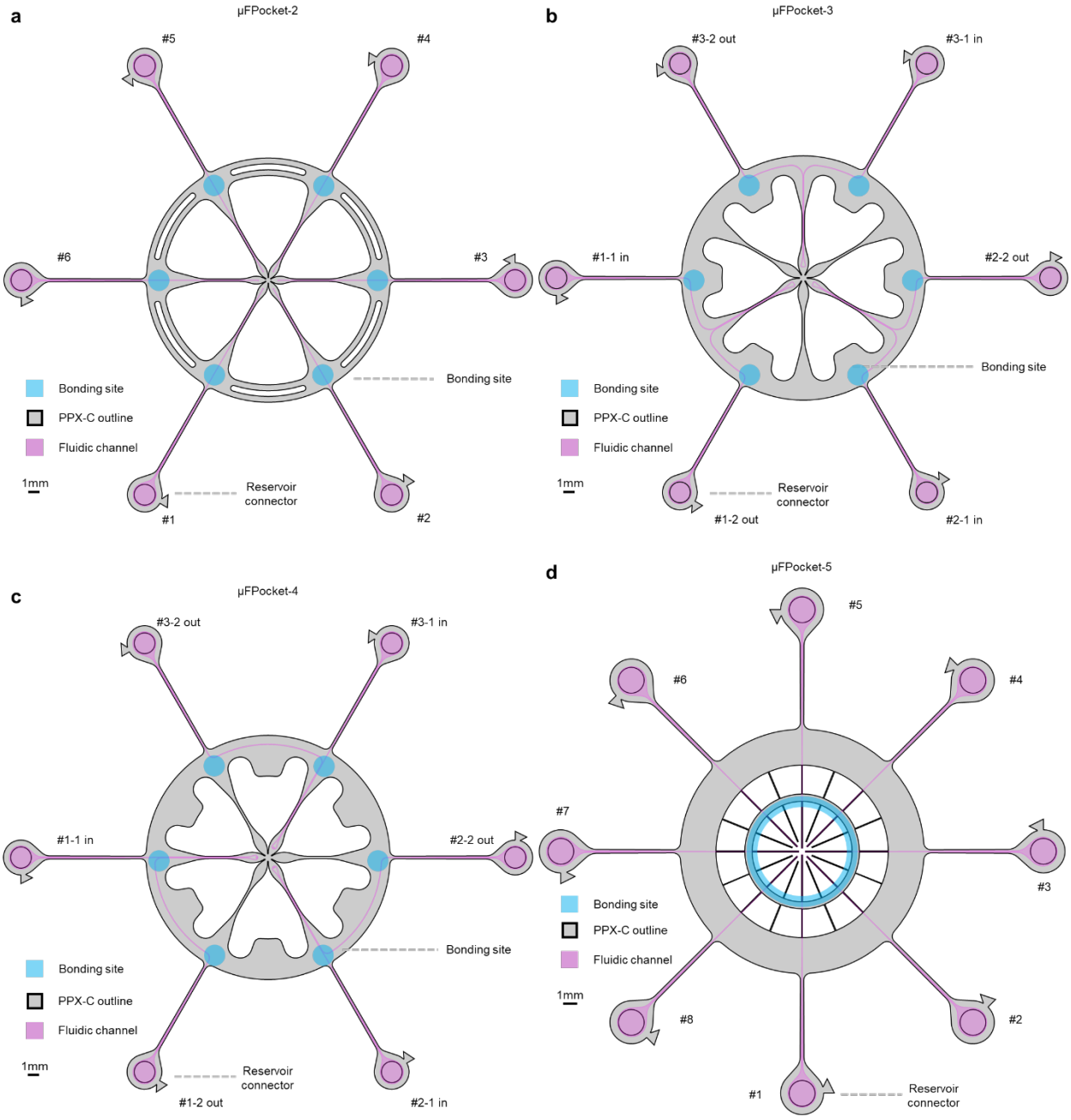

Figure S19. Two-dimensional structures of μFPocket-2, 3, 4, and 5. Layers (microfluidics and PPX-C) are labeled in different colors.

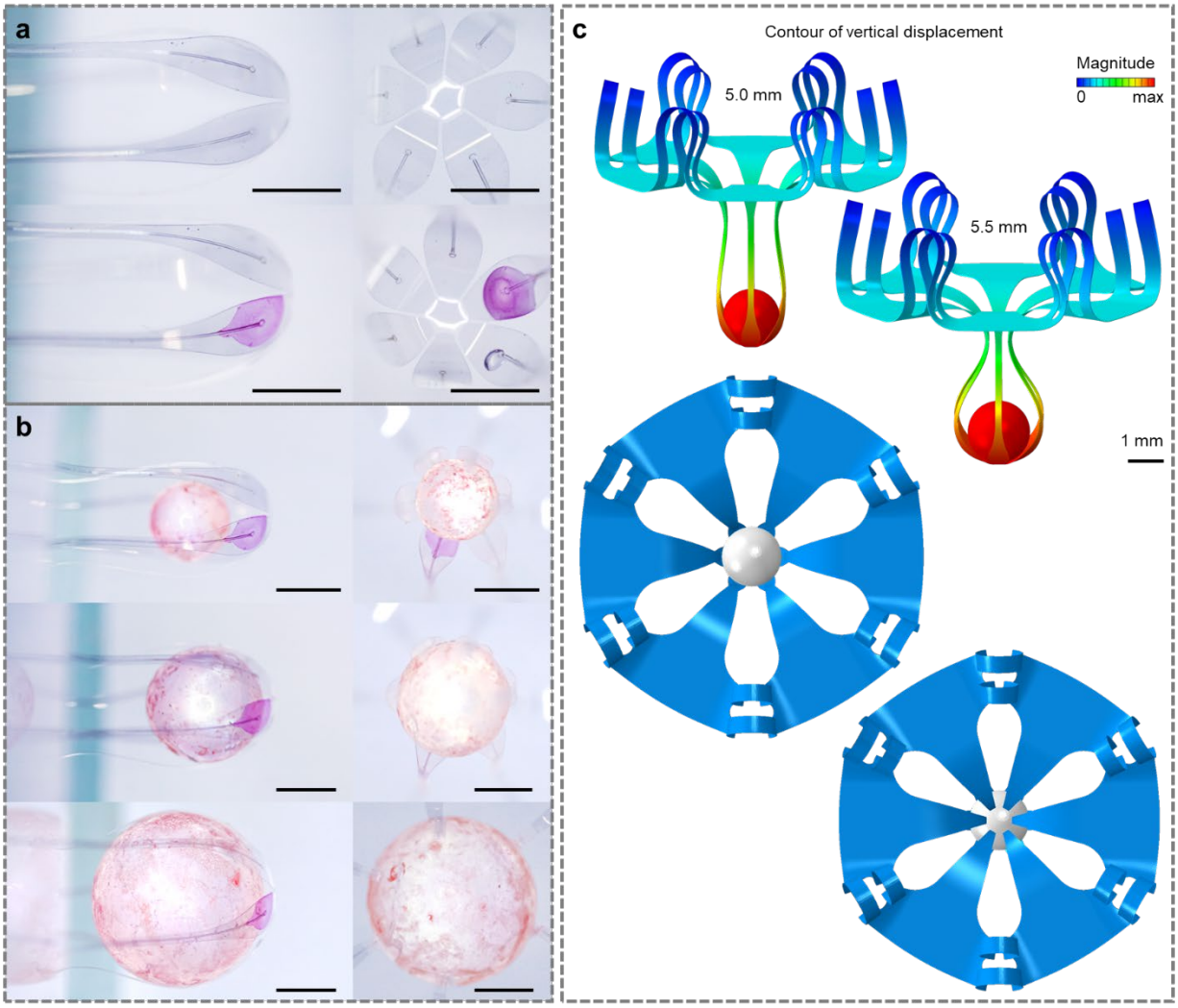

Figure S20. Structure flexibility tests of μFPocket-2. a. Optical images of 3D deterministic-folded μFPocket-2 in standby (top) and drug delivering (bottom) stages. **b.** 3D assembled μFPocket-2 holding organoid phantoms with different diameters (Φ=1.3, 2, 2.9 mm from top to bottom). **c.** FEA simulation of Fluidpocket-2 with adjustable pocket size by varying pre-stretched distance (5 and 5.5 mm). Sphere diameter is 2 mm. Scale bars: 1 mm.

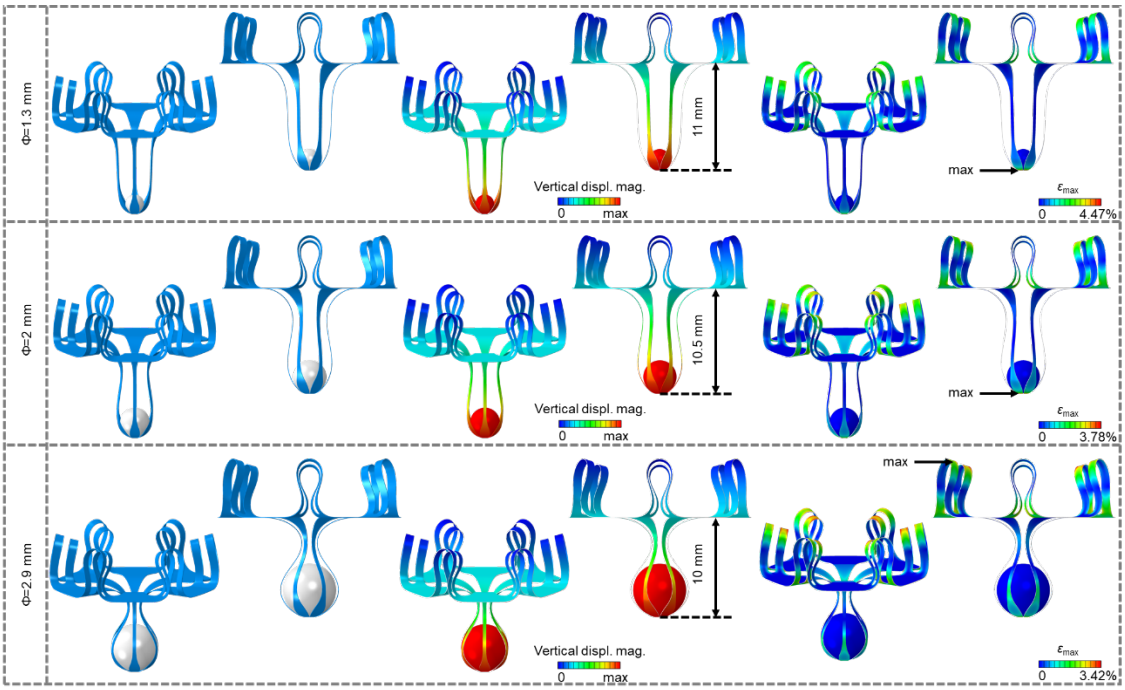

Figure S21. FEA simulation studying μFPocket-2 holding different spheres. Sphere diameters Φ=1.3, 2, 2.9 mm**.**

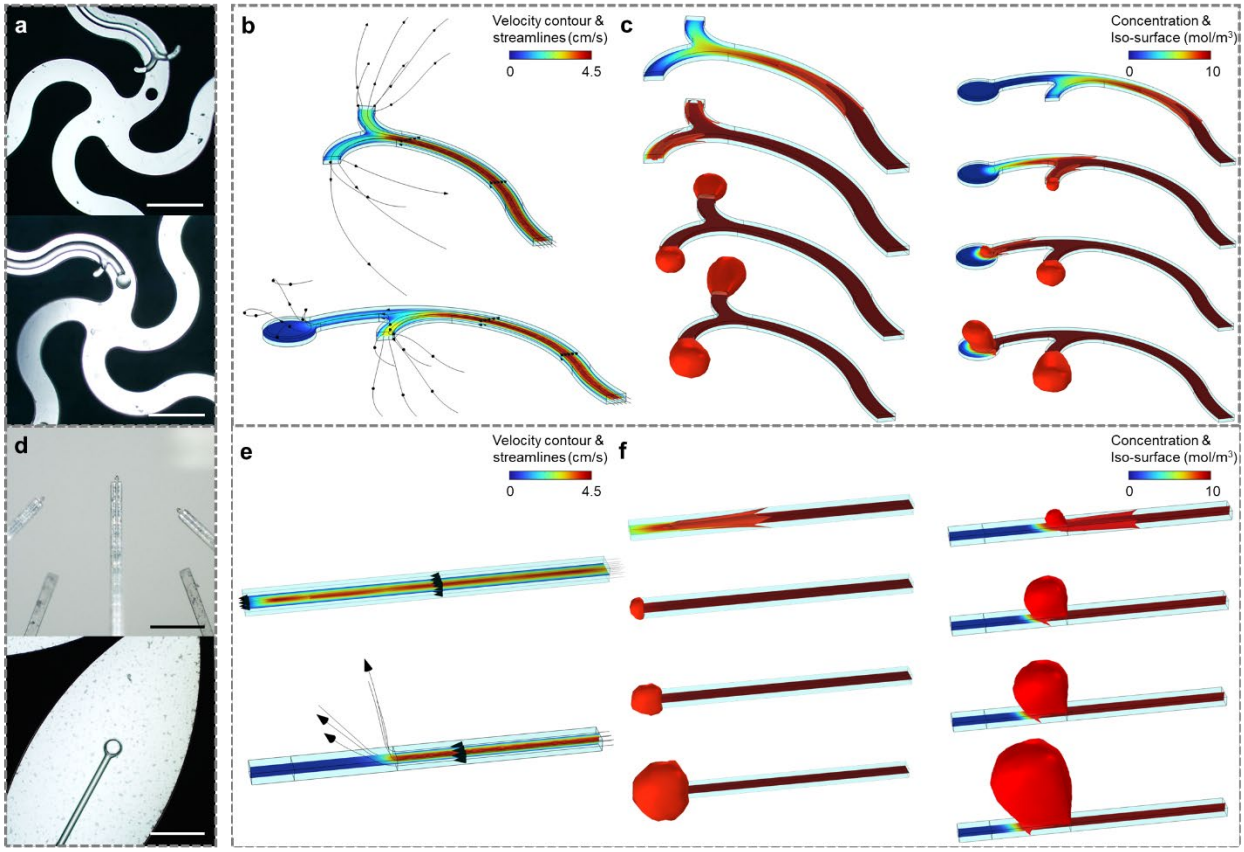

Figure S22. Outlet structures of microfluidic channel and the corresponding simulations. **a.-c.** Channel outlets of μFPocket-1. Optical images (**a**) of microfluidics outlets (top: double-side outlet; bottom: side and top outlet) are presented. **b.-c.** Velocity contours (**b**) and concentration iso-surfaces (**c**) of fluidics from the simulation. d.-f. Channel outlets of μFPocket-2 and μFPocket-5. Optical images (**d**) of microfluidics outlets (top: terminal outlet; bottom: top outlet) are presented. **e.-f.** Velocity contours (**e**) and concentration iso-surfaces (**f**) of fluidics from the simulation. Scale bars: 250 μm.

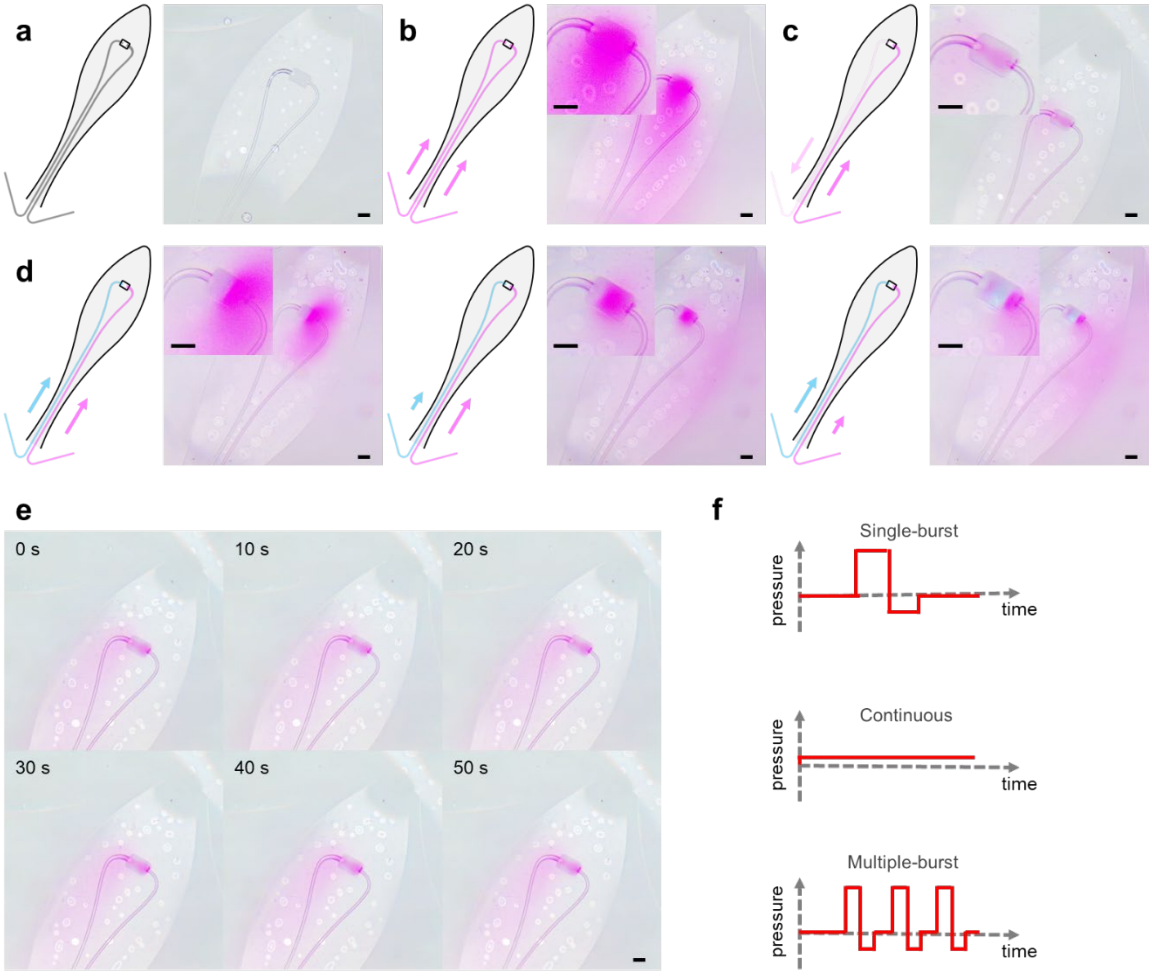

Figure S23. Outlet design for ultra-localized chemical stimulation. Schematic illustrations and optical images of different conditions are presented. **a.** Standby. **b.** 2 channels delivering drug. **c.** 1 channel delivering drug and 1 channel taking media. **d.** 2 channels delivering different drugs with adjustable flow rate. **e.** Characterization of flow stability. **f.** Schematic illustration of drug delivery modes. Scale bars: 100 μm.

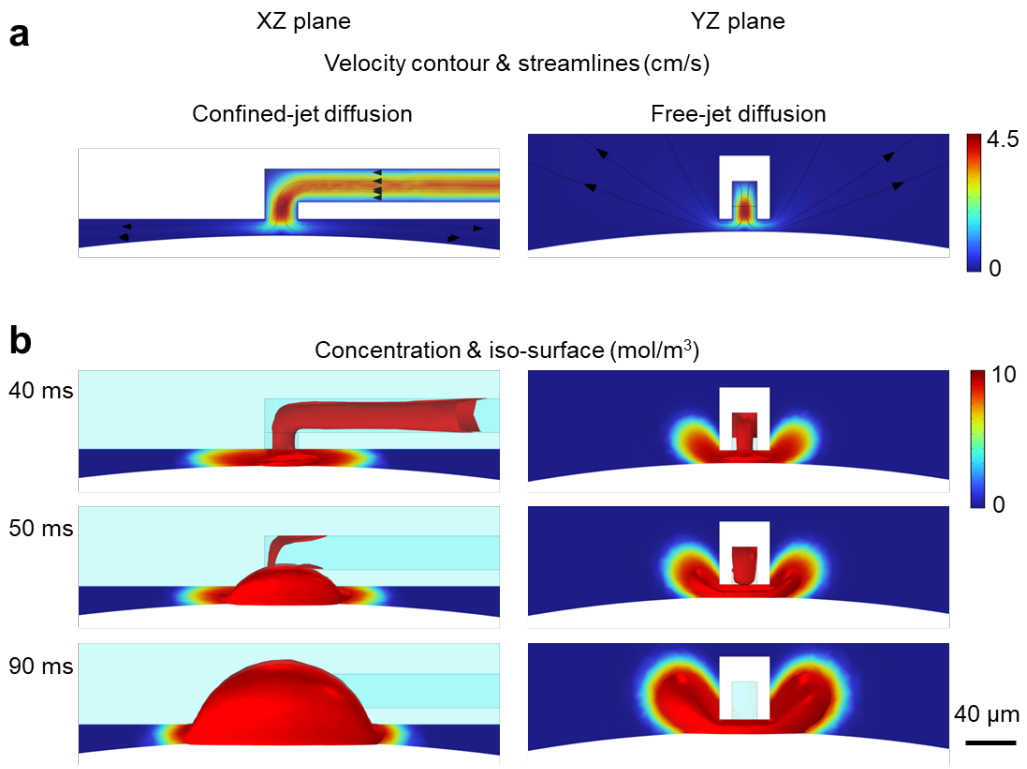

Figure S24. Simplified model of fluidic-organoid interface. Velocity contour (**a**) and concentration iso-surface (**b**) of organoid-fluidic contact interface (XZ and YZ planes) are presented. Scale bars: 40 μm.

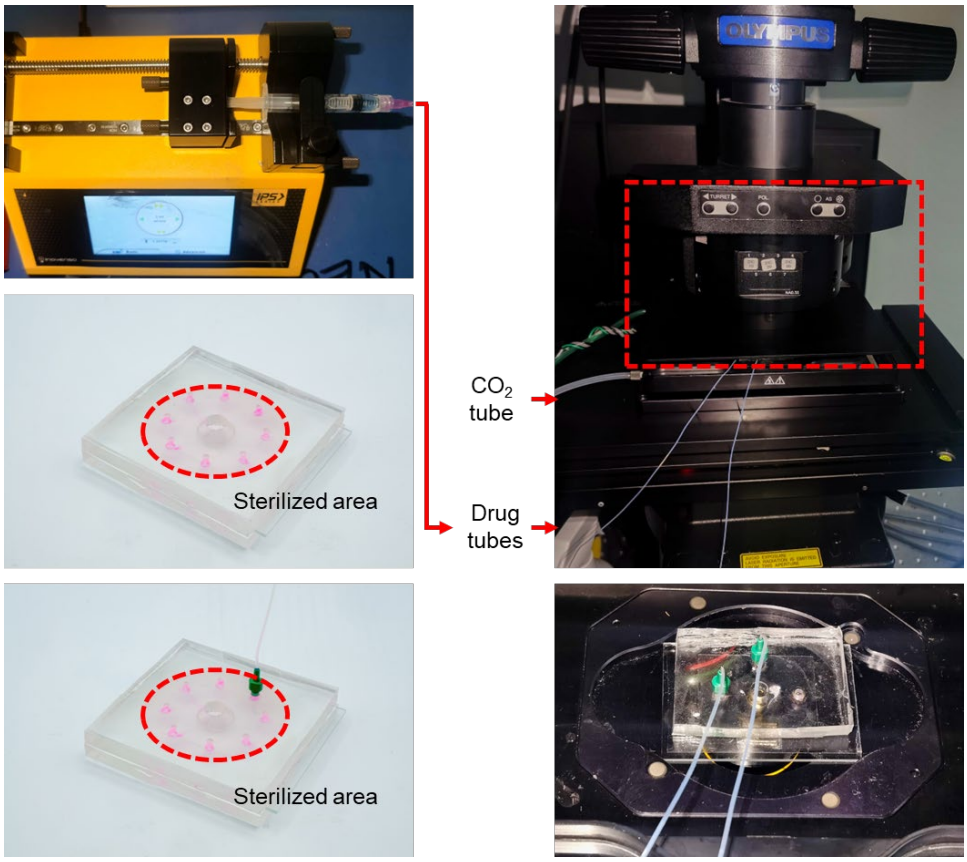

Figure S25. Experimental setup of drug delivery and in situ Ca^{2+} imaging.

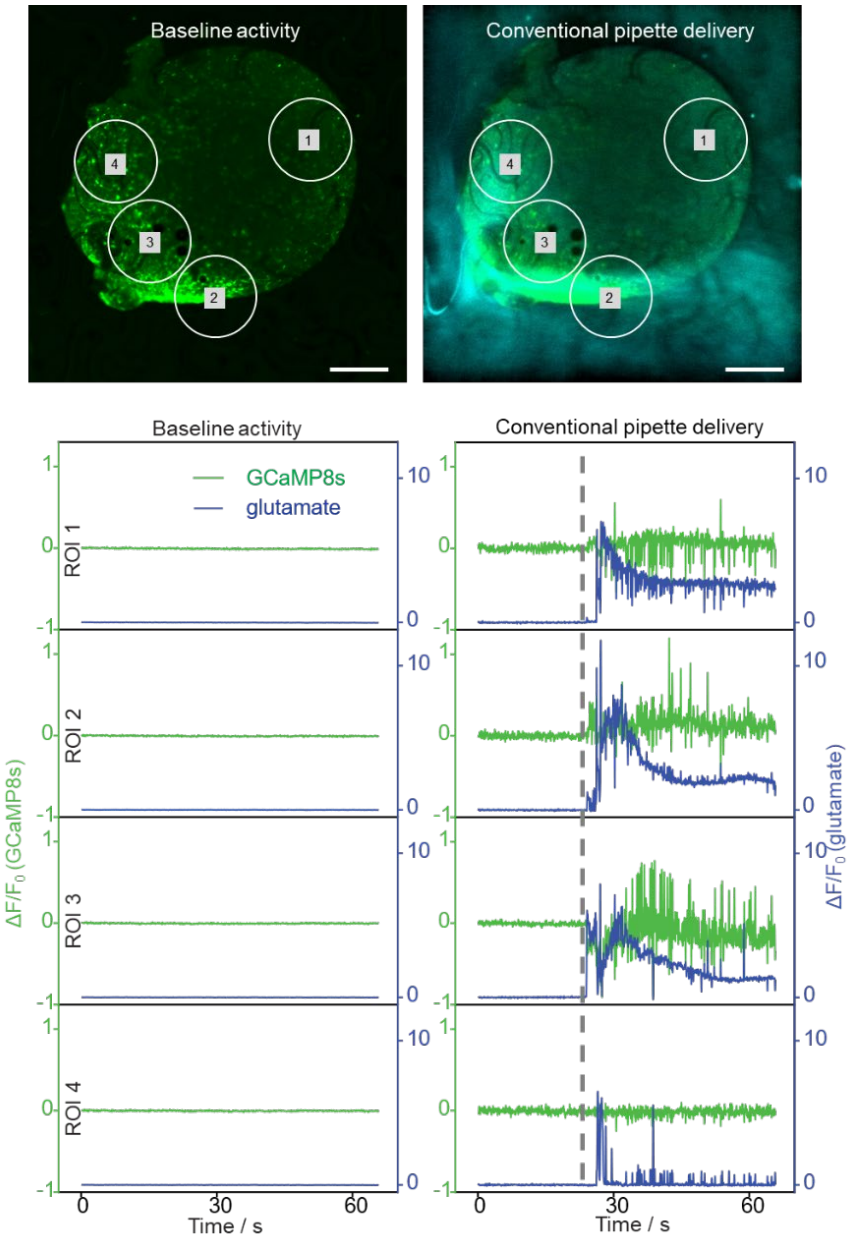

Figure S26. Quantitative fluorescence activity recording corresponding to Fig. 4. Same set of ROIs are used as in **Fig. 4e-f**. The dash line represents the time when glutamate was delivered through a pipette.

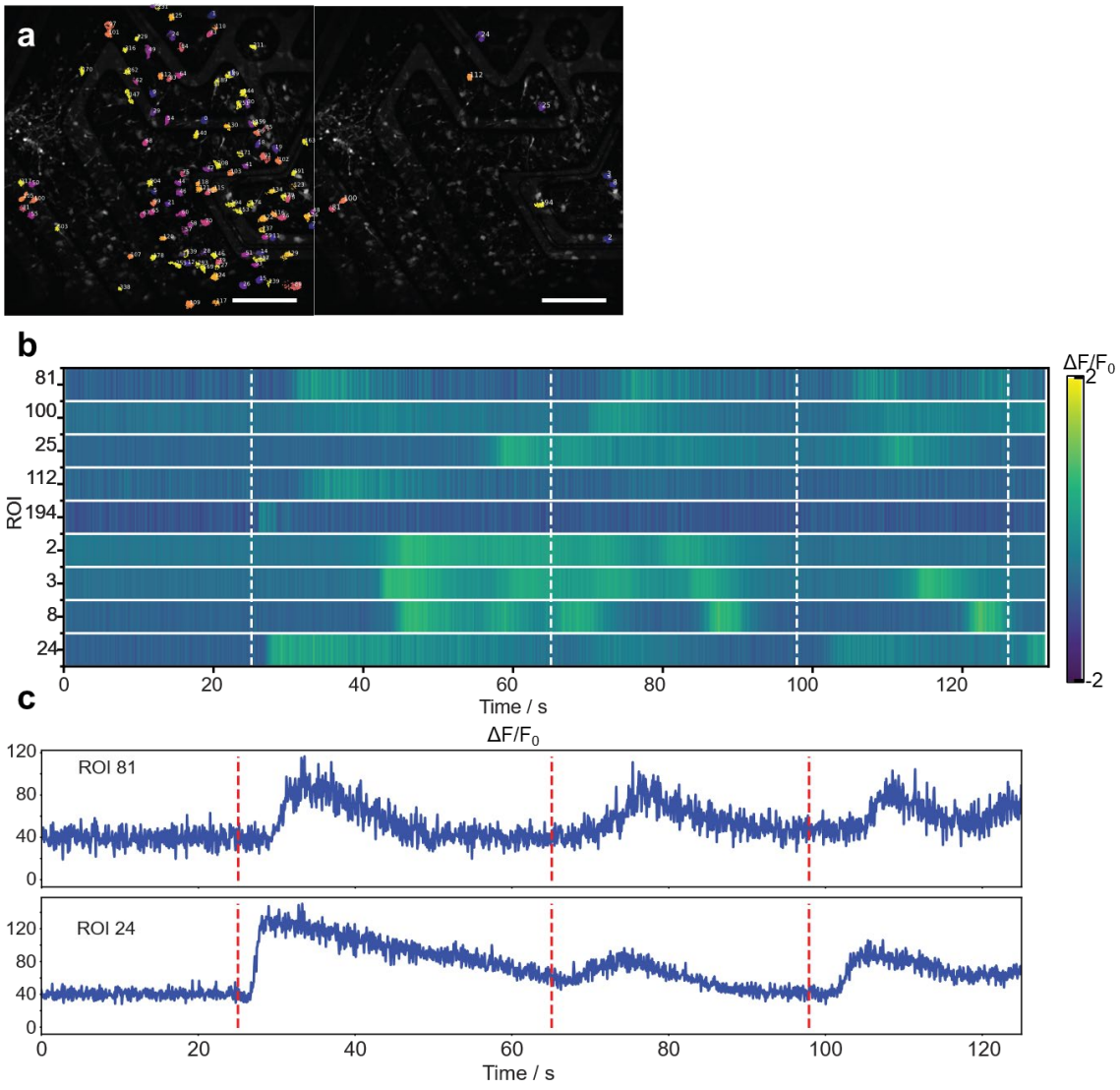

Figure S27. Activity mapping for ROIs corresponding to Fig. 6d, global stimulation. a. ROI labels of responding neurons (left) and near-electrode responding neurons (right). **b.** Fluorescence activity spectrogram of near-electrode neuron's ROIs. **c.** Typical ROIs that show synchronized fluorescence activities with electrical stimulations. White and red dash lines in **b-c** represent the time when electrical stimulations were applied. Scale bars: 200 μm.

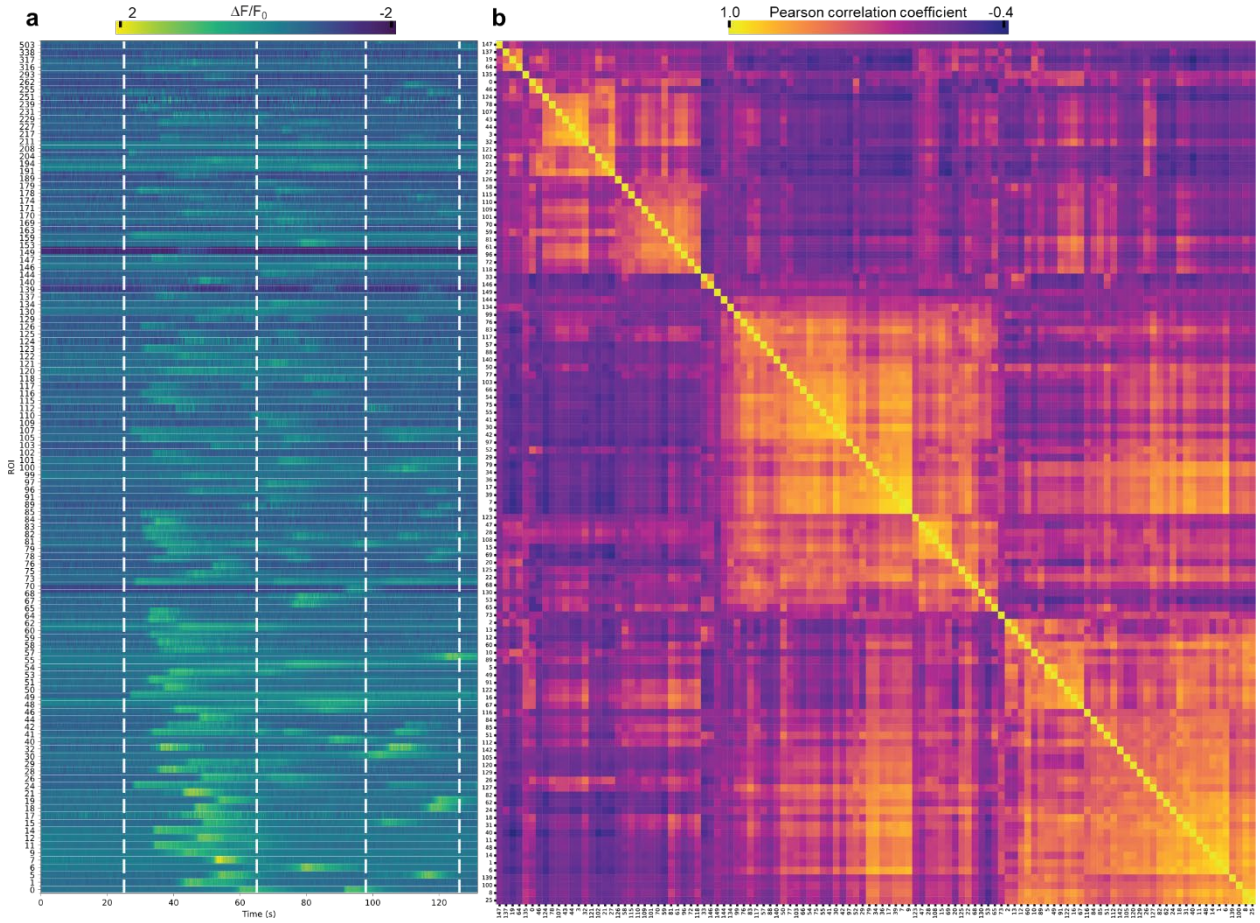

Figure S28. Activity mapping for ROIs corresponding to Fig. 6d, global stimulation. Activity heatmap (**a**) and correlation matrix (**b**) of responding ROIs are presented. White dash lines in **a** represent the time when electrical stimulations were applied.

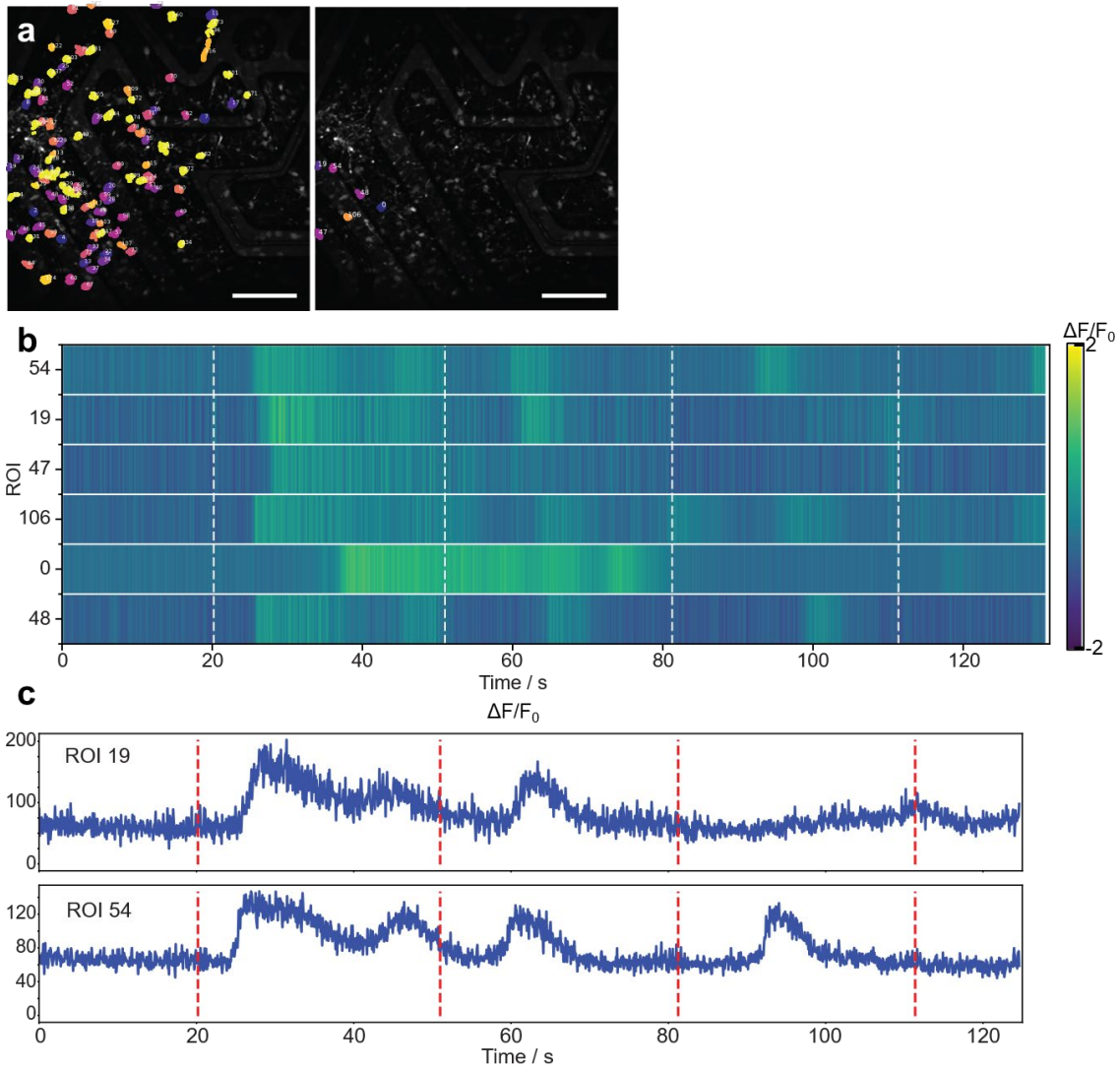

Figure S29. Activity mapping for ROIs corresponding to Fig. 6d, local stimulation. a. ROI labels of responding neurons (left) and near-electrode responding neurons (right). **b.** Fluorescence activity spectrogram of near-electrode neuron's ROIs. **c.** Typical ROIs that show synchronized fluorescence activities with electrical stimulations. White and red dash lines in **b-c** represent the time when electrical stimulations were applied. Scale bars: 200 μm.

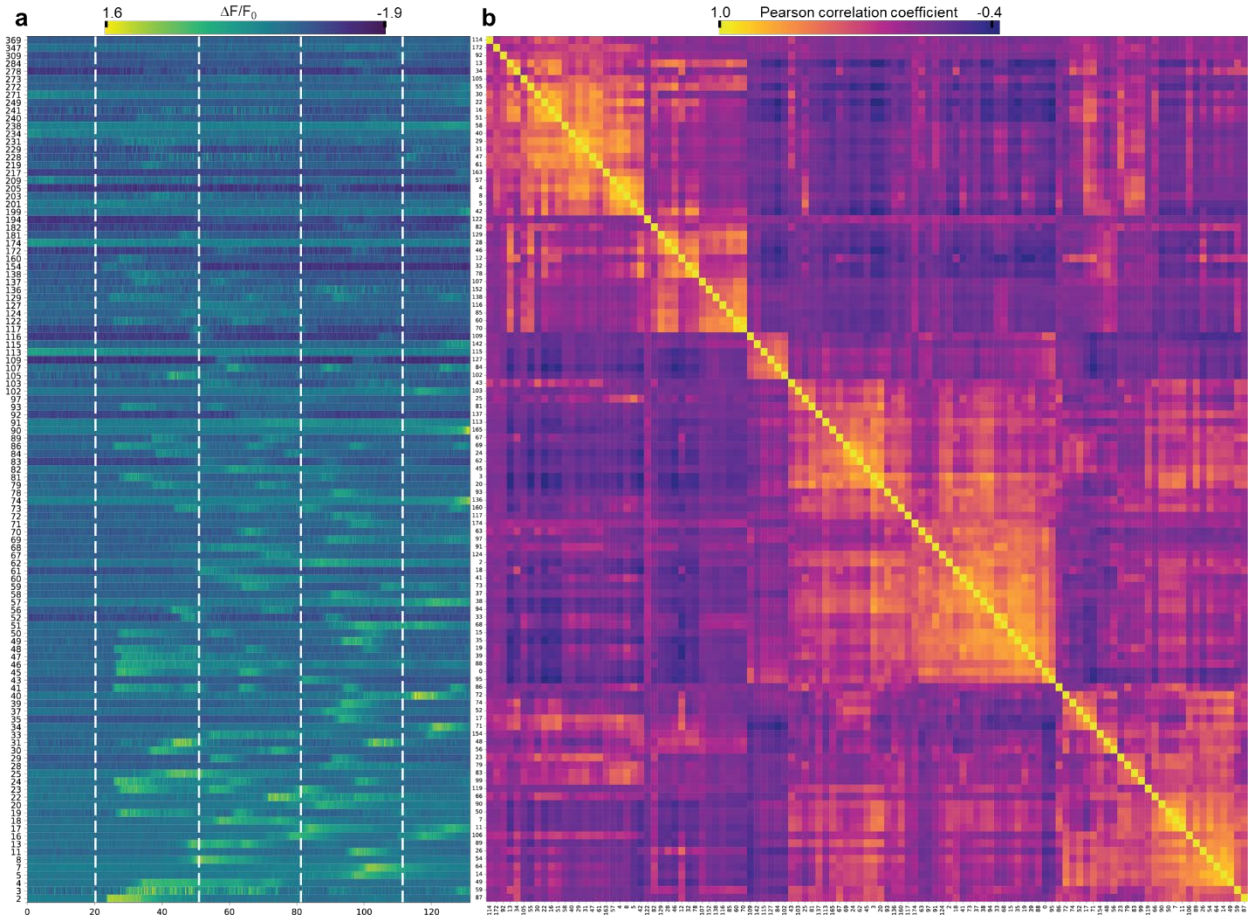

Figure S30. Activity mapping for ROIs corresponding to Fig. 6d, local stimulation. Activity heatmap (**a**) and correlation matrix (**b**) of responding ROIs are presented. White dash lines in **a** represent the time when electrical stimulations were applied.

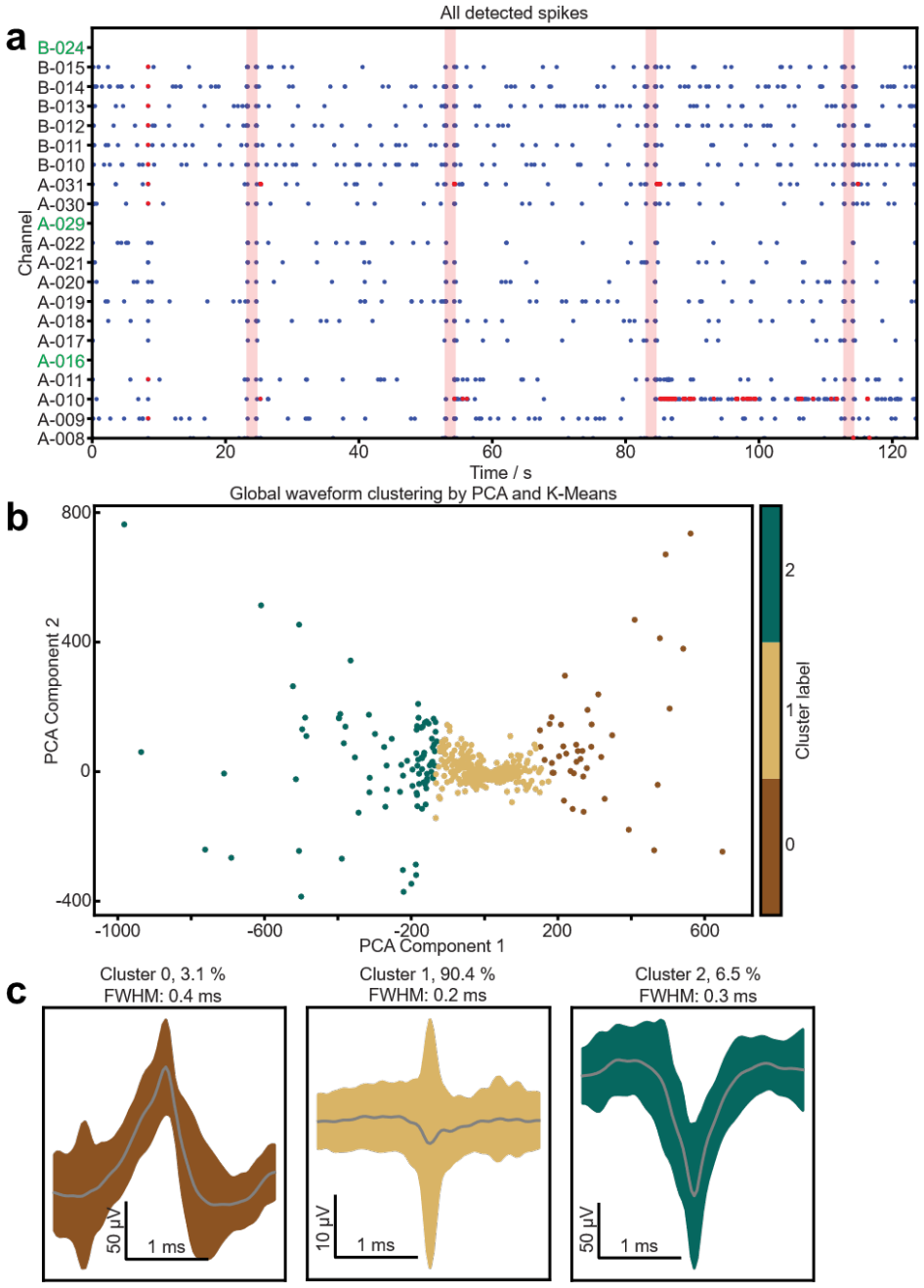

Figure S31. Spike analyses corresponding to Fig. 6g-j. a. Raster plot of spike detection. Spikes from Clusters 0 and 2 are labeled in red. **b.** PCA clustering of waveforms. **c.** Waveforms of spikes from clustering.

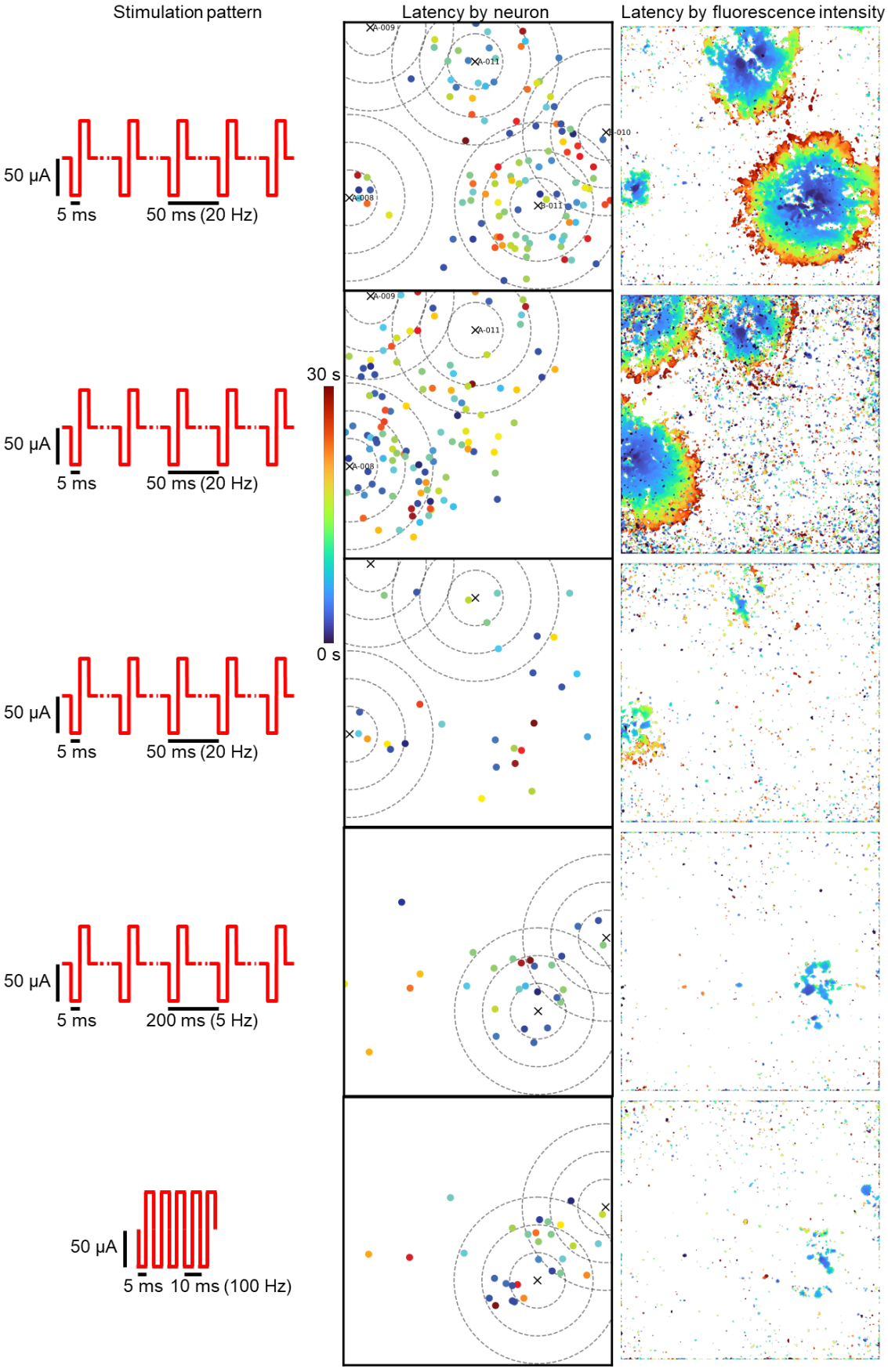
Stimulation pattern
Latency by neuron
Latency by fluorescence intensity
50 µA
5 ms
50 ms (20 Hz)
50 µA
5 ms
50 ms (20 Hz)
50 µA
5 ms
50 ms (20 Hz)
50 µA
5 ms
200 ms (5 Hz)
50 µA
5 ms
10 ms (100 Hz)
30 s
0 s
A-009
A-011
A-010
A-008
B-011

Figure S32. Average latency plots of neural activity after different stimulations.

Supplementary Movie 1. Channel Opening. The movie shows the accelerated dissolving of sacrificial microfluidic channel template, a critical step in the fabrication of μFPocket and μEFPocket precursors.

Supplementary Movie 2. μFPocket-1 Sequential Releasing. The movie shows the sequential release of Rhodamine B solution from eight separate channels of μFPocket-1 in the air.

Supplementary Movie 3. μFPocket-1 Solution Test. The movie shows a three-pulse release of Rhodamine B solution from a single channel of μFPocket-1 in water.

Supplementary Movie 4. μEFPocket-1 Solution Test. The movie shows pulse-like release of Rhodamine B solution through three separate channels of μEFPocket-1 in water.

Supplementary Movie 5. μEFTest-1 and μFTest-2 Demonstration. The movie shows the in-the-air chemical delivery functionality of folded μEFTest-1 and μFTest-2.

Supplementary Movie 6. Media Refreshing. The movie shows the media refreshing functionality using μFPocket-5.

Supplementary Movie 7. Delivering Modes Demonstration. The movie shows different chemical delivery modes using μFPocket-4.

Supplementary Movie 8. Delivery Comparison. The movie shows comparison between neural activity of the organoid by Ca imaging^{2+} under baseline condition, traditional pipette-based glutamate delivery, and glutamate delivery by μFPocket-1. GCaMP8s (green) and glutamate (cyan) channels are combined.

Supplementary Movie 9. Site-specific Glutamate Delivery. The movie shows a three-stage site-specific glutamate delivery to organoid using μFPocket-1. GCaMP8s (green), glutamate (cyan), and combined channels are shown.

Supplementary Movie 10. Multimode Delivery. The movie shows a comparison between pulse-like and continuous delivery modes using μFPocket-1. GCaMP8s (green), glutamate (cyan), and combined channels are shown.

Supplementary Movie 11. Neural Responses upon Electrical Stimulation. The movie shows a comparison between neural activity of the organoid by Ca imaging^{2+} under baseline condition and electrical stimulation by μEFPocket-1.

Supplementary Movie 12. Comparison of Different Electrical Stimulations. The movie shows a comparison between neural activity of the organoid by Ca imaging^{2+} under different stimulation conditions by μEFPocket-1.